WATERFRONT SHEET PILE WALLS SUBJECTED TO EARTHQUAKE SHAKING: ANALYSIS METHOD

Final Report on Sea Grant Project R/OE-8
Submitted to Sea Grant Program

Principal Investigator:

Toyoaki Nogami

Scripps Institution of Oceanography
University of California at SanDiego, La Jolla, CA 92093

TABLE OF CONTENTS

1. INTRODUCTION

1.1 Previous Studies Related to Seismic Earth Pressure on Retaining Walls

Seismic effects on rigid retaining walls (i.e. gravity walls) have been studied both theoretically and experimentally. Mononobe (1919) and Okabe (1926) proposed a simplified formulation to evaluate the seismic lateral earth pressure on a retaining wall backfilled with dry cohesionless naturals (Mononobe-Okabe method). Their method is based on a plastic limit condition and assumes a triangular distribution of earth pressure along the wall height. According to this pressure distribution, the total force is acting at the one-third of the wall height from the bottom. Using small scale rigid wall models with dry sand backfill, the earth pressure due to dynamic ground shaking was investigated experimentally by using a shake table (Mononobe and Matsuo, 1919; Jacobsen, 1939; Matsuo, 1941; and Ishii, Arai and Tsuchida, 1960). The experimental results showed that the maximum lateral earth pressure was roughly equal to that predicted by the Mononobe-Okabe, but the location of the total lateral force was higher than one-third of the wall height. It was also shown that the increase of the permanent lateral earth pressure after the shaking was substantially higher than the maximum dynamic transient pressure during shaking. Prakash and Basavanna (1969) and Seed and Whitman (1970) modified the Mononobe-Okabe method and assumed a more realistic distribution of earthquake lateral pressure. Sabzevari and Ghahramani (1974) used the incremental rigid plasticity theory to obtain analytical expressions and construct stress displacement and velocity fields behind the wall. This

method enables us to compute the lateral earth pressure for various types of rigid wall displacement.

Formulations based on elastic analysis were also developed for the evaluation of the dynamic lateral earth pressure. Matsuo and Ohara (1965) and Tajimi (1973) solved elastic wave equations to obtain the formulations. Scott (1973) modeled the soil and wall system as an elastic vertical shear beam and a rigid wall connected each other by distributed horizontal Winkler springs and developed the formulae to compute the dynamic earth pressure. Given earthquake excitation at the base of the beam, the beam simulates the free-field earthquake ground motion, and Winkler springs produce the soil-wall interaction force (i.e. lateral earth pressure). Those formulations based on elastic analysis generally estimate the maximum lateral earth pressure significantly higher than those estimated by the formulations based on a plastic limit condition. Elastic analysis may be justified if the lateral response of the wall is not large enough to produce a plastic limit condition behind the wall.

It depends on the displacement of the wall whether the backfill soil is in an elastic condition or plastic limit condition. The nonlinear finite element method is a convenient analysis tool to evaluate the lateral earth pressure since the conditions in the soil are automatically adjusted according to the magnitude of strains developed in the soil. Potts and Fourier (1986) used a finite element method and found that the displacement pattern of the wall highly affects the amount of the wall displacement required to fully mobilize the plastic limit condition behind the wall and the pressure distribution. Those indicate that the wall

flexibility affects the lateral earth pressure on the wall. Kuralowicz and Tejchman (1984) investigated experimentally the static earth pressure on rigid and flexible sheet-pile walls in cohesionless soil. It was observed that the distribution shape of the lateral earth pressure on a flexible wall was nonlinear, although that on a rigid wall was nearly triangular. Ayala, Romo and Gomez (1985) investigated the maximum bending moment of flexible walls induced by seismic earth pressure by using the finite element method. Flexibility of the wall was found to affect the maximum moment.

Kurata, Arai and Yokoi (1965) conducted shaking table tests with a small scale anchored sheet-pile wall model in dry cohesionless soil. They observed that the ground shaking increased the lateral earth pressure substantially in the vicinity of the anchor level but did not increase much in the middle part of the wall. This is due to redistribution of the lateral earth pressure resulting from flexural deformation of the wall. The total lateral earth pressure observed during shaking was smaller than that computed by the Mononobe-Okabe method. It was also observed that the increase of permanent lateral earth pressure due to the permanent soil deformation was much larger than the transient dynamic earth pressure. Murphy (1960) also conducted model tests on an anchored sheet-pile wall subjected to earthquake shaking. It was pointed out that the wall translated outward without tilting until the anchor pull failed. As essentially planar slip surface was observed in the backfill soil. Similar planer slip surface was observed by Bolton and Steedman (1985).

When the backfill soil is submerged, a portion of the water in the pores of the soil mass moves with the lateral soil skeleton (restrained water)

and the other portion moves freely during ground shaking (free water). The hydrodynamic pressure in the backfill against the wall is due to the motion of the free water, and this depends on the volume of the free water. Anzo (1936) formulated the hydrodynamic pressure in the submerged backfill against the wall. The formulation was based on a rigid soil skeleton, Darcy's flow and Navier-Stokes equations. According to this formulation, the hydrodynamic pressure in the soil never exceeds the value computed by Westergard's formula and is smaller for a lower permeability. Matsuo and Ohara (1965) conducted model tests on the wall with submerged backfill sand. The observed hydrodynamic pressure was somewhat larger than that computed by Westergard's formula. Liquefaction was observed in some of those tests. Ishibashi, Matsuzawa and Kawamura (1985) proposed the method estimate the dynamic pressure against the wall retaining submerged backfill soil. The method adopts the Mononobe-Okabe method (with the soil weight increased by the restrained water weight) for earth pressure and simplified Anzo's formula for hydrodynamic pressure.

Towhata and Islam (1987) viewed that the magnitude of permanent wall displacement was the most critical phenomena for the judgement of the degree of seismic damage of anchored bulkheads. Based on this view, they developed a simple method to compute the lateral movement of anchored bulkheads induced by earthquake shaking assuming a triangular sliding wedge behind the wall. They considered that the effect of liquefaction in backfill was particularly important and thus was taken into account in the method.

1.2 Observation of Earthquake Damages to Waterfront Sheet Pile Walls

The Niigata earthquake in 1964 caused substantial damages to retaining structures. Most of those damages were closely connected to the development of excess pore water pressure associated with liquefaction process.

The ministry of Transportation (1964) published a detailed report on earthquake damages in Niigata harbor facilities. The report indicates that substantial translation of walls occurred toward the water at the wall next to Yamanoshota Wharf, due to loose reclaimed backfills. The North and South Wharfs were suffered from excessive two-meter movement of their walls. Similar movement was detected in the Bandai-Jima area as well. The North bank of the Shinano River completely collapsed, accompanied by overall displacement of backfill toward the river. Although the report concluded that most sheet-pile wall damages were due to tilting, it also mentioned that lateral translation took place in walls of shallow embedment. At the areas of all those anchored bulkheads, evidences of liquefaction were reported.

1.3 Objective of the Study

The objective of the project is to develop an analysis tool for computing the behavior and conditions of waterfront sheet pile walls during and right after the earthquake ground shaking. Key factors for the judgement of the seismic performance of waterfront anchor bulkheads are bending moment in the wall and permanent lateral movement of wall, induced by

earthquake shaking. According to the previous section, those are affected mainly by elastic and inelastic soil behavior, excess porewater pressure, flexibility of wall, motions of backfill and wall, and hdro-dynamic pressure at both front and back sides of the wall. The finite element method may be the most convenient analysis method to consider rationally all of those important factors affecting the performance of walls, and thus was developed in the project.

Fig. 1.1 shows finite element models of a waterfront sheet pile wall. The effect of water at the front side of the wall is taken into account by added masses attached at the nodes located at the water-wall and water-soil interfaces. Those masses are active for motions only in the component normal to the interface. Soil elements are formulated treating the soil mass as a water-saturated two phase mixture. This enables soil elements to simulate the coupling between porewater motions and soil frame motions, generation and dissipation of excess porewater pressure in a soil mass, and effects of excess porewater pressure on the soil frame behavior. Discontinuity of displacements develops at the soil-wall interface due to large difference in the stiffnesses between those of the wall and soil and due to sliding and separation between the wall and soil. This requires special elements, termed joint elements, to accomodate such behaviors at the interface.

2. FINITE ELEMENT FORMULATION

2.1 Soil Elements

Submerged soil is treated as a fluid-saturated porous medium. The nonlinear behavior is implemented in the stress-strain relationship of the soil frame.

(1) Definitions of Valuables

Porosity n is defined as

$$n = \frac{V_f}{V_f + V_s} \tag{2.1}$$

where V_f = volume or pores or fluid; and V_s = volume of solid.
Relation given in Eq. 1 can be transformed to density relationship as

$$\rho = (1 - n)\rho_s + n\rho_f \tag{2.2}$$

where ρ, ρ_s and ρ_f= mass densities of solid-fluid mixture, solid and fluid, respectively. In order to describe the deformation of a mixture, deformations of the two phases are identified separately. The components of deformation of the solid can be denoted by u_i (i = 1, 2, 3) and components of displacement of the fluid can be denoted by U_i(i = 1, 2, 3): i denotes coordinate axes. The amount of fluid displaced from the solid skeleton, Q_i, is obtained as

$$Q_i = A_i n(U_i - u_i) \tag{2.3}$$

where A_i = area of mixture normal to the ith direction.

The displacement of fluid relative to solid skeleton, averaged over the face of the mixture is obtained as

$$W_i = \frac{Q_i}{A_i} = n(U_i - u_i) \tag{2.4}$$

The strains in the solid skeleton are defined as

$$\varepsilon_{ij} = \frac{1}{2}(u_{i,j} + u_{j,i}) \tag{2.5a}$$

or

$$\{\varepsilon\} = [L]\{u\} \tag{2.5b}$$

where

$$\{\varepsilon\}^T = \{\varepsilon_{11}\ \varepsilon_{22}\ \varepsilon_{33}\ \varepsilon_{21}\ \varepsilon_{23}\ \varepsilon_{31}\}$$

$$[L]^T = \begin{bmatrix} \frac{\partial}{\partial x_1} & 0 & 0 & \frac{\partial}{\partial x_2} & 0 & \frac{\partial}{\partial x_3} \\ 0 & \frac{\partial}{\partial x_2} & 0 & \frac{\partial}{\partial x_1} & \frac{\partial}{\partial x_3} & 0 \\ 0 & 0 & \frac{\partial}{\partial x_3} & 0 & \frac{\partial}{\partial x_2} & \frac{\partial}{\partial x_1} \end{bmatrix}$$

The change of fluid volume stored per unit volume of the mixture is given by

$$\xi = w_{i,i} \tag{2.5a}$$

or

$$\xi = \{\nabla\}^T \{w\} \tag{2.6b}$$

where

$$\{\nabla\}^T = \left[\frac{\partial}{\partial x_1} \quad \frac{\partial}{\partial x_2} \quad \frac{\partial}{\partial x_3}\right]$$

$$\{w\}^T = \left[w_1 \quad w_2 \quad w_3\right]$$

(2) Constitutive Relationship for Porous Material

The total stress is applied to the mixture as defined before and is decomposed into two parts as

$$\sigma_{ij} = \sigma'_{ij} + p\delta_{ij} \tag{2.7}$$

where σ_{ij}' = effective stress; and p = pore pressure.

Eq. 2.7 can be written in an incremental form as

$$d\sigma_{ij} = d\sigma'_{ij} + \delta_{ij}\, dp \tag{2.8}$$

Similarly, strains are also decomposed into two parts. Part of the strain is caused by deformation of grains due to pore pressure, and the part is caused by deformation of grains and skeleton due to effective stress. This can be expressed as

$$\varepsilon_{ij} = (\varepsilon_{ij})_p + (\varepsilon_{ij})_{\sigma'} \tag{2.9}$$

Strains in the solid grains induced by pore pressure can be expressed by using the bulk modulus for solid as

$$(\varepsilon_{ij})_p = \frac{p}{3K_s}\delta_{ij} \tag{2.10}$$

Deformation of solid skeleton caused by the effective stress σ_{ij}' is related to $(\varepsilon_{ij})_{\sigma'}$ through the constitutive terms or D_{ijkl}

$$\sigma_{ij}' = D_{ijkl}\,(\varepsilon_{ij})_{\sigma'} \tag{2.11}$$

Combining Eqs. 7 through 11, the following relations are obtained:

$$\begin{aligned}\sigma_{ij} &= D_{ijkl}(\varepsilon_{ij})_{\sigma'} + p\delta_{ij} \\ &= D_{ijkl}(\varepsilon_{ij}) - D_{ijkl}(\varepsilon_{ij})_p + p\delta_{ij} \\ &= D_{ijkl}\,\varepsilon_{kl} - \frac{p}{3K_s}D_{ijkl}\,\delta_{kl} + p\delta_{ij}\end{aligned} \tag{2.12}$$

which is rearranged as

$$\sigma_{ij} = D_{ijkl}\,\varepsilon_{kl} + ap\delta_{ij} \tag{2.13}$$

where

$$a = 1 - \frac{\delta_{ij} D_{ijkl} \delta_{kl}}{9K_s} \tag{2.14}$$

Continuity of fluid flow will be formulated in order to obtain a relation for pore pressure taking into the volumetric change of each phase. The total volume change of the mixture, ε_{ii}, consists of the sum of the following parts:

(1) Amount of fluid flowing out of ξ, (= change of volume of pores);

(2) Volume change in solid due to p, (= $p(1-n)/K_s$);

(3) Volume change due to p, (= np/K_f); and

(4) volume change of solid due to effective stress, $\overline{\sigma} = \sigma_{ii}'/3$

Thus, the continuity condition is formulated as

$$\varepsilon_{ii} = \frac{p}{K_s}(1-n) + \frac{np}{K_f} + \frac{\dot{\sigma}_{ii}}{3K_s} - \xi \tag{2.15}$$

Rewriting σ'_{ii} in Eq. 2.15 with Eqs. 2.9, 2.10 and 2.11 leads to

$$\varepsilon_{ii} = \left\{\frac{1-n}{K_s} + \frac{n}{K_f}\right\} p + \frac{1}{3K_s}\left\{D_{iikl}\varepsilon_{kl} - D_{iikl}(\varepsilon_{ij})_p\right\} - \xi$$

$$= \left\{\frac{1-n}{K_s} + \frac{n}{K_f}\right\} p + \frac{1}{3K_s} D_{iikl}\varepsilon_{kl} - \frac{1}{3K_s} D_{iikl} \frac{\delta_{kl}}{3K_s} p - \xi$$

or

$$p = Q(\xi + a\varepsilon_{kk}) \tag{2.16}$$

where

$$\frac{1}{Q} = \frac{n}{K_f} + \frac{a-n}{K_s} \tag{2.17}$$

Equations for constitutive relation of porous material are summarized as

$$\sigma_{ij} = D_{ijkl}\,\varepsilon_{kl} + ap\delta_{ij} \tag{2.13}$$

$$p = Q(\xi + a\varepsilon_{kk}) \tag{2.16}$$

$$a = 1 - \frac{\delta_{ij} D_{ijkl} \delta_{kl}}{9K_s} \tag{2.14}$$

$$\frac{1}{Q} = \frac{n}{K_f} + \frac{a-n}{K_s} \tag{2.17}$$

For nonlinear behavior, the constitutive relation needs to be expressed in incremental form. The incremental forms of Eqs. 2.13 and 2.16 are

$$d\sigma_{ij} = D^t_{ijkl}\, d\varepsilon_{kl} + a^t\, dp\, \delta_{ij} \tag{2.18}$$

$$dp = Q^t(d\xi + a^t\, d\varepsilon_{kk}) \tag{2.18}$$

where

$$a^t = 1 - \frac{\delta_{ij} D^t_{ijkl} \delta_{kl}}{9K_s} \tag{2.20}$$

and D^t_{ijkl} is incremental constitutive tensor for skeleton. The value a^t is nearly equal to 1 since the second term at the right hand side of Eq. 20 is very small compared with the first term (Zienkeiewicz at al., 1984). Eqs. 2.18 and 19 with a = 1 can be rewritten in a matrix form as

$$\{d\sigma\} = [D]^{ep} \{d\varepsilon\} + \{r\}\, dp \tag{2.21}$$

$$dp = Q\left[\{r\}^T \{d\varepsilon\} + d\xi\right] \tag{2.22}$$

where

$$\frac{1}{Q} = \frac{n}{K_f} + \frac{1-n}{K_s} \tag{2.23}$$

and

$$\{d\sigma\}^T = \{d\sigma_{11}\ d\sigma_{22}\ d\sigma_{33}\ d\sigma_{12}\ d\sigma_{23}\ d\sigma_{31}\}$$
$$\{d\varepsilon\}^T = \{d\varepsilon_{11}\ d\varepsilon_{22}\ d\varepsilon_{33}\ d\varepsilon_{12}\ d\varepsilon_{23}\ d\varepsilon_{31}\} \tag{2.24}$$

$$\{r\}^T = \{1\ \ 1\ \ 1\ \ 0\ \ 0\ \ 0\}$$

(3) Dynamic Equilibrium Equation

Two equations are required to describe the equilibrium conditions of two phase mixture. We will look at the equilibrium conditions in the

mixture as a whole and in the fluid phase first. Masses of a solid phase and fluid phase in a unit volume of mixture are respectively $(1-n)\rho_s$ and $n\rho_f$. Therefore, the equilibrium conditions in mixture as a whole are described as

$$\sigma_{ij,j} + (1-n)\rho_s b_i + n\rho_f b_i - (1-n)\rho_s \ddot{u}_i - n\rho_f \ddot{U}_i = 0 \qquad (2.25)$$

where b_i = ith component of body force per unit mass; $\ddot{u} = \partial^2 u/\partial t^2$; and $\ddot{U} = \partial^2 U/\partial t^2$. The equilibrium conditions of fluid phase will be developed from the generalized Darcy's equation described by

$$\dot{w} = n(\dot{U} - \dot{u}) = k_{ij}\, h_{,j} \qquad (2.26)$$

where $\{\dot{w}\ \dot{U}\ \dot{u}\} = \partial(w\ U\ u)/\partial t$; k_{ij} = component of permeability tensor; h_{ij} = gradient of fluid head in the jth direction. Under the steady state conditions, the gradient of the head is composed of pressure gradient, body force gradient and inertia of fluid. This is written as

$$h_{,j} = p_{,i} + \rho_f b_i - \rho_f \ddot{U}_i \qquad (2.27)$$

Combining Eqs. 2.26 and 2.27, equilibrium conditions in fluid phase can be described as

$$p_{,i} + \rho_f b_i = \rho_f \ddot{U}_i + k_{ij}^{-1} n(\dot{U}_i - \dot{u}_i) \qquad (2.28)$$

Substitution of $\rho_f U_i$ in Eq. 2.28 into Eq. 2.25 yields

$$\sigma_{ij,j} + \rho b_i - (1-n)\rho_s \ddot{u}_i + k_{ij}^{-1} n^2 (\dot{U}_i - \dot{u}_i) - n p_{,i} - n\rho_f b_i = 0 \qquad (2.29)$$

Using σ_{ij} expressed by Eq. 2.7, Eq. 2.29 results in equilibrium condition in solid skeleton expressed as

$$\sigma'_{ij,j} + (1-n)p_{,i} + (1-n)\rho_s b_i - (1-n)\rho_s \ddot{u}_i + k_{ij}^{-1} n^2 (\dot{U}_i - \dot{u}_i) = 0 \qquad (2.30)$$

Hereafter, Eqs. 2.30 and 2. 28 will used for two equilibrium equations for two phase mixture. Those will be rewritten in a matrix form as

$$[L]^T\{\sigma'\} + (1-n)\{\nabla\}^T p + (1-n)\rho_s\{b\} - (1-n)\rho_s\{\ddot{u}\} + n^2[k]^T\left(\{\dot{U}\} - \{\dot{u}\}\right) = 0 \qquad (2.31)$$

$$\{\nabla\}^T p + \rho_f\{b\} - \rho_f\{\ddot{U}\} - n[k]^T\{\dot{U} - \dot{u}\} = \{0\} \qquad (2.32)$$

(4) Finite Element Formulation for Numerical Evaluation

The principle of virtual work requires that for an arbitrary virtual displacement, the work done through Eqs. 2.31 and 2.32 over the domain of interest must be equal to zero. This requirement on Eq. 2.31 is given by

$$\int_\Omega \{\delta u\}^T\left([L]^T\{\sigma'\} + (1-n)\{\nabla\}^T p + (11-n)\rho_s\{b\} - (1-n)\rho_s\{\ddot{u}\} + n^2[k]^T\{\dot{U} - \dot{u}\}\right) d\Omega = 0 \qquad (2.33)$$

where Ω = the domain of interest; $\{\delta u\}$ = components of virtual displacement compatible with $\{u\}$. Similarly, application of virtual work principle to Eq. 2.32 results in

$$\int_{\Omega} \{\delta u\}^T \left(n\{\nabla\}^T p + n\rho_f \{b\} - n\rho_f \{\dot{U}\} - n^2 [k]^T \{\dot{U}\} + n^2 [k]^T \{\dot{u}\} \right) d\Omega = 0 \qquad (2.34)$$

where $\{\delta U\}$ = components of virtual displacement compatible with $\{U\}$. Using Gauss's theorem, Eqs. 2.33 and 2.34 can be reduced to

$$\int_{\Omega} \left([L]^T \{\delta u\} \right)^T \{\sigma'\} \, d\Omega - \int_{\Gamma} \{\delta u\}^T \{T\} \, d\Gamma + (1-n) \int_{\Omega} \left(\{\nabla\}^T \{\delta u\} \right)^T p \, d\Omega -$$

$$(1-n) \int_{\Gamma} \{\delta u\}^T \{\hat{p}\} \, d\Gamma - (1-n)\rho_s \int_{\Omega} \{\delta u\}^T \{b\} \, d\Omega + (1-n)\rho_s \int_{\Omega} \{\delta u\}^T \{\ddot{u}\} \, d\Omega -$$

$$n^2 \int_{\Omega} \{\delta u\}^T [k]^T \{\dot{U} - \dot{u}\} \, d\Omega = 0 \qquad (2.35)$$

$$n \int_{\Omega} \left(\{\nabla\}^T \{\delta U\} \right)^T p \, d\Omega - n \int_{\Gamma} \{\delta U\}^T \{\hat{p}\} \, d\Gamma - n\rho_f \int_{\Omega} \{\delta U\}^T \{b\} \, d\Omega +$$

$$n\rho_f \int_{\Omega} \{\delta U\}^T \{\ddot{U}\} \, d\Omega + n^2 \int_{\Omega} \{\delta U\}^T [k]^T \{\dot{U} - \dot{u}\} \, d\Omega = 0 \qquad (2.36)$$

where $\{T\}$ = components of surface traction in equilibrium with stresses at the boundary such that

$$[\sigma] \{r\} = \{T\} \qquad (2.37)$$

in which $\{r\}$ = components of unit vector normal to the boundary Γ; and $\{\hat{p}\}$ = pore pressure at the boundary expressed as

$$\{\hat{p}\} = \{r\} p \qquad (2.38)$$

The domain is divided into finite elements. Within an element, the variables are approximated in terms of the values of variables at nodal points such that

$$\{u\} = [N]\{\bar{u}\}, \quad \{U\} = [N]\{\bar{U}\} \tag{2.39}$$

where [N] = matrix of interpolation function for {u} and {U}; $\{\bar{u}\}$ and $\{\bar{U}\}$ = vectors of nodal variables of {u} and {U}, respectively. Then, since [N] is function of spatial coordinates only, it is also approximated that

$$\begin{aligned} \{\ddot{u}\} &= [N]\{\ddot{\bar{u}}\}, \ \{\dot{U}\} = [N]\{\dot{\bar{U}}\} \\ \{\dot{u}\} &= [N]\{\dot{\bar{u}}\}, \ \{\dot{U}\} = [N]\{\dot{\bar{U}}\} \end{aligned} \tag{2.40}$$

Similarly, {δu} and {δU} are approximated by

$$\{\delta u\} = [N]\{\delta\bar{u}\}, \ \{\delta U\} = [N]\{\delta\bar{U}\} \tag{2.41}$$

Using ξ defined by Eq. 2.6a with {w} = n{U-u}, Eq. 2.22 can be rewritten as

$$\begin{aligned} dp &= Q\left(\{r\}^T\{d\varepsilon\} + d\xi\right) \\ &= Q\left(\{r\}[L]\{du\} + n\{\nabla\}^T\{dU\} - n\{\nabla\}^T\{du\}\right) \\ &= Q(1-n)\{\nabla\}^T\{du\} + Qn\{\nabla\}^T\{dU\} \end{aligned} \tag{2.42}$$

Substitution of Eq. 2.42 and Eqs. 2. 39 through Eq. 2.41 into Eqs.2. 35 and 2.36 leads to

$$[M_u]\{\ddot{\bar{u}}\} + [C_1]\{\dot{\bar{u}}\} - [C_1]\{\dot{\bar{U}}\} + \int_{\Omega}[B_u]^T\{\sigma\}\, d\Omega + [K_1]\{\bar{u}\} + [K_2]\{\bar{U}\} = \{f_u\} \quad (2.43)$$

$$[M_U]\{\ddot{\bar{U}}\} - [C_1]^T\{\dot{\bar{u}}\} + [C_1]\{\dot{\bar{U}}\} + [K_2]^T\{\bar{u}\} + [K_3]\{\bar{U}\} = \{f_U\} \quad (2.44)$$

where

$$[M_u] = (1-n)\rho_s \int_{\Omega}\{N\}^T[N]\, d\Omega$$

$$[M_U] = n\rho_f \int_{\Omega}[N]^T[N]\, d\Omega$$

$$[C_1] = n^2 \int_{\Omega}[N]^T[k]^T[N]\, d\Omega$$

$$[K_1] = (1-n)^2 Q \int_{\Omega}\left(\{\nabla\}^T[N]\right)^T\{\nabla\}^T[N]\, d\Omega$$

$$[K_2] = (1-n)nQ \int_{\Omega}\left(\{\nabla\}^T[N]\right)^T\{\nabla\}^T[N]\, d\Omega$$

$$[K_3] = n^2 Q \int_{\Omega}\left(\{\nabla\}^T[N]\right)^T\{\nabla\}^T[N]\, d\Omega$$

$$\{f_u\} = (1-n)\rho_s \int_{\Omega}[N]^T\{b\}\, d\Omega + \int_{\Gamma}[N]^T\{t\}\, d\Gamma + (1-n)\int_{\Gamma}[N]^T\{\hat{p}\}\, d\Gamma$$

$$\{f_U\} = n\rho_f \int_{\Omega}[N]^T\{b\}\, d\Omega + n\int_{\Gamma}[N]^T\{\hat{p}\}\, d\Gamma$$

$$[B_u] = [L]^T[N]$$

Combining Eqs. 2.43 and 2.44, we have

$$\begin{bmatrix} M_u & 0 \\ 0 & M_U \end{bmatrix}\begin{Bmatrix} \ddot{\bar{u}} \\ \ddot{\bar{U}} \end{Bmatrix} + \begin{bmatrix} C_1 & -C_1^T \\ -C_1^T & C_1 \end{bmatrix}\begin{Bmatrix} \dot{\bar{u}} \\ \dot{\bar{U}} \end{Bmatrix} + \begin{bmatrix} K'+K_1 & K_2 \\ K_2^T & K_3 \end{bmatrix}\begin{Bmatrix} \bar{u} \\ \bar{U} \end{Bmatrix} = \begin{Bmatrix} f_u \\ f_U \end{Bmatrix} \qquad (2.45)$$

or

$$[M]\{d\ddot{v}\} + [C]\{d\dot{v}\} + [K]\{dv\} - [\phi]\{d\bar{\lambda}\} = \{df\} \qquad (2.46)$$

where

$$[M] = \begin{bmatrix} M_u & 0 \\ 0 & M_U \end{bmatrix}$$

$$[C] = \begin{bmatrix} C_1 & -C_1^T \\ -C_1^T & C_1 \end{bmatrix}$$

$$[K] = \begin{bmatrix} K'+K_1 & K_2 \\ K_2^T & K_3 \end{bmatrix}$$

$$[\phi] = \begin{bmatrix} \phi_0 & 0 \\ 0 & 0 \end{bmatrix}$$

$$[K'] = \int_{\Omega} [B]^T[D][B_u]\, d\Omega$$

$$[\phi_0] = \int_\Omega [B_u]^T \left[\frac{\partial \{g\}^T}{\partial \{\sigma\}}\right]^T [D]\, d\Omega$$

$$\{dv\} = \begin{Bmatrix} d\bar{u} \\ d\bar{U} \end{Bmatrix}$$

$$\{df\} = \begin{Bmatrix} df_u \\ df_U \end{Bmatrix}$$

$$\{d\bar{\lambda}\} = \begin{Bmatrix} d\bar{\lambda} \\ 0 \end{Bmatrix}$$

Incremental equation of equilibrium can be written as

$$[M]\{\Delta d\ddot{v}\} + [C]\{\Delta d\dot{v}\} + [K]\{\Delta dv\} - [\phi]\{d\bar{\lambda}\} = \{\Delta df\} \qquad (2.45)$$

(5) Stress-Strain Constitutive Equation

Elasto-plastic behavior is considered in the stress-strain relationship of the porous skeleton. In this report four different yield criteria, the Trescas, Von Mises, Mohr-Coulomb and Drucker-Prager criteria, are employed. The latter two are applicable to concrete, rocks and soils.

It is assumed that the following requirements are met:

1. An explicit relationship between stress and strain must be formulated to describe material behavior under elastic conditions, i.e. before the onset of plastic deformation.
2. A yield criterion indicating the stress level at which plastic flow comments must be postulated.
3. A relationship between stress and strain must be developed for post yield behavior, i.e. when the deformation is made up of both elastic and plastic components.

Before the onset of plastic yielding, the relationship between stress and strain is given by the standard linear elastic expression.

$$\sigma_{ij} = D_{ijkl}\,\varepsilon_{kl} \tag{2.80}$$

where D_{ijkl} = tensor of elastic constant. For an isotropic material, D_{ijkl} is expressed in the form of

$$D_{ijkl} = \lambda\delta_{ii}\delta_{kl} + \mu\delta_{ik}\delta_{jl} + \mu\delta_{ii}\delta_{jk} \tag{2.81}$$

where λ and μ =Lame's constants; and δ_{ij} = Kronecker delta defined by

$$\delta_{ij} = \begin{cases} 1 & \text{if } i = j \\ 0 & \text{if } i \neq j \end{cases} \tag{2.82}$$

a. Yield Criteria

The yield criterion determines the stress level at which plastic deformation begins. With the stress invariants defined by

$$J_1 = \sigma_{ii}$$
$$J_2 = \frac{1}{2}\sigma_{ij}\,\sigma_{ij} \qquad (2.84)$$
$$J_3 = \frac{1}{3}\sigma_{ij}\,\sigma_{jk}\sigma_{kl}$$

the yield criterion can be written in the form of

$$f(J_2', J_3') = S(s) \qquad (2.85)$$

where f and S = some functions to be determined experimentally; s = hardening parameter; J_2' and J_3' = the second and third invariants of the deviatoric stresses expressed by

$$\sigma_{ij}' = \sigma_{ij} - \frac{1}{3}\delta_{ij}\sigma_{kk} \qquad (2.86)$$

Tresca yield criterion: This states that the yielding begins when the maximum shear stress reaches to a certain value or

$$\sigma_1 - \sigma_3 = S(s) \qquad (2.87)$$

for $\sigma_1 \geq \sigma_2 \geq \sigma_3$ where σ_1, σ_2, and σ_3 = principle stresses.

Von Mises yield criterion: This states that yielding occurs when J_2' reaches to a value

$$(J_2')^{\frac{1}{2}} = S(s) \qquad (2.88)$$

The second deviatoric stress invariant, J_2', can be explicitly written as

$$J_2' = \frac{1}{6}\left\{(\sigma_1 - \sigma_2)^2 + (\sigma_2 - \sigma_3)^2 + (\sigma_3 - \sigma_1)^2\right\}$$

$$= \frac{1}{2}\left\{(\sigma_x')^2 + (\sigma_y')^2 + (\sigma_z')^2\right\} + \tau_{xy}^2 + \tau_{yz}^2 + \tau_{xz}^2 \qquad (2.89)$$

Yield criteria, Eq. 2.88 may be further written as

$$\bar{\sigma} = \sqrt{3}\, S(s) \qquad (2.90)$$

where $\bar{\sigma}$ is termed effective stress, generalized stress or equivalent stress, expressed as

$$\bar{\sigma} = \sqrt{3}\,(J_2')^{\frac{1}{2}} = \sqrt{\frac{3}{2}}\,\{\sigma_{ij}'\,\sigma_{ij}'\}^{\frac{1}{2}} \qquad (2.91)$$

Mohr-Coulomb yield criteria: This is a generalization of the Coulomb friction failure law defined by

$$\tau = c - \sigma_n \tan\phi \qquad (2.93)$$

where τ and σ_n = shear and normal stresses, respectively; c = cohesion; and ϕ = internal friction angle. For $\sigma_1 > \sigma_2 > \sigma_3$, Eq. 2.93 can be rewritten as

$$\frac{1}{2}(\sigma_1 - \sigma_3)\cos\phi = c - \left(\frac{\sigma_1+\sigma_3}{2} - \frac{\sigma_1-\sigma_3}{2}\sin\phi\right)\tan\phi \qquad (2.94)$$

or rearranging

$$(\sigma_1 - \sigma_3) = 2c\cos\phi - (\sigma_1+\sigma_3)\sin\phi \qquad (2.95)$$

Drucker-Prager yield criterion: This is a modification of the Von Mises yield criterion for making it dependent on hydrostatic pressure like the Mohr-Coulomb criteria. The influence of a hydrostatic stress component on

yielding was introduced by inclusion of an additional term in the Von Mises expression given

$$\alpha J_1 + (J_2')^{\frac{1}{2}} = S \tag{2.96}$$

The yield surface defined by Eq. 2.96 in the principal stress space is a circular cone whereas that defined by the Mohr-Coulomb is a conical yield surface whose normal section is an irregular hexagon. The following expressions for α and S makes the Drucker-Prager circle coincide with the outer apices of the Mohr-Coulomb hexagon at any section:

$$\alpha = \frac{2 \sin \phi}{\sqrt{3}\,(3 - \sin \phi)} \tag{2.97}$$

$$S = \frac{6c \cos \phi}{\sqrt{3}\,(3 - \sin \phi)} \tag{2.98}$$

Coincidence with the inner apices of the Mohr-Coulomb hexagon is provided by

$$\alpha = \frac{2 \sin \phi}{\sqrt{3}\,(3 + \sin \phi)} \tag{2.99}$$

$$S = \frac{6c \cos \phi}{\sqrt{3}\,(3 + \sin \phi)} \tag{2.100}$$

b. Work or Strain Hardening

If f = s represents a yield surface, the elastic and plastic conditions exist respectively when f < s and f = s. At plastic state, the

incremental change in the yield function due to an incremental stress change is

$$df = \frac{\partial f}{\partial \sigma_{ij}} d\sigma_{ij} \qquad (2.\ 105)$$

Then if:

$df < 0$ elastic unloading occurs (elastic behavior) and the stress point returns inside the yield surface.

$df = 0$ neutral loading (plastic behavior for a perfect plastic material) and stress point remains on the yield surface.

$df > 0$ plastic loading (plastic behavior for a strain hardening material) and the stress point remains on the expanding yield surface.

c. Elasto-Plastic Stress-Strain Relationship

After initial yielding the material behavior will be partly elastic and partly plastic. During any increment of stress, the changes of strain are assumed to be divisible into elastic and plastic components such that

$$d\varepsilon_{ij} = (d\varepsilon_{ij})_e + (d\varepsilon_{ij})_p \qquad (2.106)$$

The elastic strain increment is related to the stress increment by Eq. 2.80. Decomposing the stress terms into their deviatoric and hydrostatic components, the elastic component of the incremental strain can be expressed as

$$\frac{d\bar{\sigma}}{d\bar{\varepsilon}_p} = H'(\bar{\varepsilon}_p) \tag{2. 114}$$

For the uniaxial case ($\sigma_1 = \sigma$, $\sigma_2 = \sigma_3 = 0$), Eq. 2.91 leads to incremental effective stress and effective strain expressed respectively as

$$d\bar{\sigma} = \sqrt{\frac{2}{3}} \{d\sigma_{ij}' \, d\sigma_{ij}'\}^{\frac{1}{2}} = d\sigma \tag{2.115}$$

$$d\bar{\varepsilon} = \sqrt{\frac{2}{3}} \{(d\varepsilon_{ij}')_p \, (d\varepsilon_{ij}')_p\}^{\frac{1}{2}} = d\varepsilon_p \tag{2.116}$$

Substitution of Eqs. 2.115 and 2.116 into Eq. 2.114 leads to

$$H' = \frac{d\sigma}{d\varepsilon_p} = \frac{d\sigma}{d\varepsilon - d\varepsilon_e} = \frac{1}{\frac{d\varepsilon}{d\sigma} - \frac{d\varepsilon_e}{d\sigma}} = \frac{E^T}{1 - \frac{E^T}{E}} \tag{2.117}$$

where E^T = tangent modulus. Thus, the hardening function H' = can be determined experimentally from a simple uniaxial yield test.

Adopting the strain hardening hypothesis, Eq. 2. 85 can be rewritten as

$$F(\sigma, s) = f(\sigma) - S(s) = 0 \tag{2.121}$$

Differentiating Eq. 2.121, we have

$$dF = \frac{\partial F}{\partial \sigma} d\sigma + \frac{\partial F}{\partial s} ds = 0 \tag{2.122}$$

or

$$\{a\}^T\{d\sigma\} - A\, d\bar{\lambda} = 0 \tag{2.123}$$

where

$$\{a\}^T = \left(\frac{\partial F}{\partial \sigma_x}, \frac{\partial F}{\partial \sigma_y}, \frac{\partial F}{\partial \sigma_z}, \frac{\partial F}{\partial \tau_{yz}}, \frac{\partial F}{\partial \tau_{zx}}, \frac{\partial F}{\partial \tau_{xy}} \right) \tag{2.124}$$

$$A = \frac{1}{d\bar{\lambda}} \frac{\partial F}{\partial s} ds \tag{2.125}$$

The vector {a} is termed the flow vector.

Eq. 2.112 can be rewritten as

$$\{d\varepsilon\} = [D]^{-1}\{d\sigma\} + d\bar{\lambda}\left\{\frac{\partial F}{\partial \sigma}\right\}^T \tag{2.126}$$

Premultiplying both sides of Eq. 2.126 by $\{a\}^T[D]$ and eliminating $\{a\}^T ds$ by use of Eq. 2.123, the plastic multiplier $d\bar{\lambda}$ can be expressed as

$$d\bar{\lambda} = \frac{1}{A + \{a\}^T[D]\{a\}} \{a\}^T[D]\{d\varepsilon\} \tag{2.127}$$

Substitution of Eq. 2.127 into Eq. 2.126, with $dD^T = a^T D$ and $dD = Da$, results in

$$d\sigma = D^{ep}\, d\varepsilon \tag{2.128}$$

where

$$D^{ep} = D - \frac{dD\, dD^T}{A + dD^T a} \tag{2.129}$$

The uniaxial conditions, $\sigma_1 = \sigma$ and $\sigma_2 = \sigma_3 = 0$, are considered. With work hardening hypothesis, ds is

$$ds = \sigma^T d\varepsilon_p \tag{2.130}$$

Eq. 2.125 can be rewritten for uniaxial condition as

$$A = \frac{1}{d\bar{\lambda}} \frac{d\sigma}{ds} ds \tag{2.131}$$

Employing the normality condition in Eq. 2.130 results in

$$ds = d\lambda\, a^T \sigma \tag{2.132}$$

Eq. 2.124 for uniaxial condition is

$$\frac{d\sigma}{d\varepsilon_p} = H' \tag{2.133}$$

Using Euler's theorem applicable to all homogeneous function of order one, we have

$$\frac{\partial f}{\partial \sigma} \sigma = \sigma \tag{2.134}$$

or

$$a^T \sigma = \sigma \tag{2.135}$$

Substituting Eqs. 2.133 and 2.135 into Eqs. 2.132 and 2.131, $\bar{\lambda}$ and A are found to be

$$d\bar{\lambda} = d\varepsilon_p \tag{2.136}$$

$$A = H' \tag{2. 137}$$

Thus, A is the second slope of the uniaxial stress-strain curve and can be determined experimentally from Eq. 2. 117.

It is written as

$$\sin 3\theta = -\frac{3\sqrt{3}}{2}\frac{J_3}{(J_2')^{\frac{3}{2}}} \tag{2.138}$$

Then, the total principal stresses can be expressed by

$$\begin{Bmatrix}\sigma_1\\ \sigma_2\\ \sigma_3\end{Bmatrix} = \frac{2(J_2')^{\frac{1}{2}}}{\sqrt{3}}\begin{Bmatrix}\sin(\theta+\frac{2\pi}{3})\\ \sin\theta\\ \sin(\theta+\frac{4\pi}{3})\end{Bmatrix} + \frac{J_1}{3}\begin{Bmatrix}1\\ 1\\ 1\end{Bmatrix} \tag{2.139}$$

The focus yield criteria can now be rewritten in terms of J_1, J_2' and θ as follows:

Tresca yield criterion

$$2(J_2')^{\frac{1}{2}} = \sigma(s) \tag{2.140}$$

Von Mises yield criterion

$$\sqrt{3}\,(J_2') = \sigma(s) \tag{2.141}$$

Mohr-Coulomb yield criterion

$$\frac{1}{3}J_1 \sin\phi + (J_2')^{\frac{1}{2}} (\cos\theta - \frac{1}{\sqrt{3}} \sin\theta \sin\phi) = c \cos\phi \tag{2.142}$$

Drucker-Prager yield criterion

$$\alpha J_1 + (J_2')^{\frac{1}{2}} = S \tag{2.143}$$

where α and S are given in Eqs. 2.97 through 2.100.

In order to calculate the Dep matrix given in Eq. 2.129, it is required to express the flow vector a and the elasticity matrix D in a form suitable for numerical computation. The explicit form of the elasticity matrix D for plane strain condition can be written as

$$[D] = \frac{E(1-\nu)}{(1+\nu)(1-2\nu)} \begin{bmatrix} 1 & N & 0 & N \\ N & 1 & 0 & N \\ 0 & 0 & \frac{N}{2\nu}-N & 0 \\ N & N & 0 & 1 \end{bmatrix} \tag{2.144}$$

where $N = \nu/(1-\nu)$. The flow vector a for plane strain condition can be written as

$$\{a\}^T = \left\{ \frac{\partial F}{\partial \sigma_x}, \frac{\partial F}{\partial \sigma_y}, \frac{\partial F}{\partial \tau_{xy}}, \frac{\partial F}{\partial \sigma_z} \right\} \tag{2.146}$$

The specific form of the vector, {a}, is given by

$$\{a\} = C_1\{a_1\} + C_2\{a_2\} + C_3\{a_3\} \tag{2.147}$$

where

$$\{a_1\}^T = \{1, 1, 0, 1\}$$

$$\{a_2\}^T = \frac{1}{2(J_2')^{\frac{1}{2}}} \{\sigma_x', \sigma_y', 2\tau_{xy}, \sigma_z'\} \tag{2.148}$$

$$\{a_3\}^T = \left\{\sigma_y'\,\sigma_z' + \frac{J_2'}{3},\ \sigma_x'\,\sigma_z' + \frac{J_2'}{3},\ -2\sigma_z'\,\tau_{xy}\,(\sigma_x'\,\sigma_y' - \tau_{xy}^2 + \frac{J_2'}{3})\right\}$$

and the deviatoric stress invariants are

$$J_2' = \frac{1}{2}\left((\sigma_x')^2 + (\sigma_y')^2 + (\sigma_z')^2\right) + \tau_{xy}^2 \tag{2.149}$$

$$J_3' = \sigma_2'\left((\sigma_z')^2 - J_2'\right) \tag{2.150}$$

The constants C1, C2 and C3 are to define the yield surface and are given as follows:.

Tresca yield criterion

$$C_1 = 0$$

$$C_2 = 2\cos\theta\,(1 + \tan\theta\tan 3\theta) \tag{2.151}$$

$$C_3 = \frac{\sqrt{3}}{J_2'}\frac{\sin\theta}{\cos 3\theta}$$

Von Mises yield criterion

$$C_1 = 0$$
$$C_2 = \sqrt{3} \qquad (2.152)$$
$$C_3 = 0$$

Mohr-Coulomb yield criterion

$$C_1 = \frac{1}{3}\sin\phi$$
$$C_2 = \cos\theta\left((1 + \tan\theta\tan 3\theta) + \frac{\sin\phi}{\sqrt{3}}(\tan 3\theta - \tan\theta)\right) \qquad (2.153)$$
$$C_3 = \frac{\sqrt{3}\sin\theta + \cos\theta\sin\phi}{2J_2'\cos 3\theta}$$

Drucker-Prager yield criterion

$$C_1 = \alpha$$
$$C_2 = 1.0 \qquad (2.154)$$
$$C_3 = 0$$

The vector, dD, in D^{ep} (Eq. 2.129) for plane strain condition is written as

$$dD = \begin{Bmatrix} d_1 \\ d_2 \\ d_3 \end{Bmatrix} = M_1 \begin{Bmatrix} a_1 \\ a_2 \\ a_3 \end{Bmatrix} + M_2 \begin{Bmatrix} 1 \\ 1 \\ 1 \end{Bmatrix} \qquad (2.155)$$

where

$$M_1 = \frac{E}{1+\nu}$$
$$M_2 = \frac{E\nu(a_1 + a_2 + a_3)}{(1+\nu)(1-2\nu)} \qquad (2.156)$$

2.2 Joint Element at Soil-Wall Interface

A discontinuity of the displacements develops at the soil-wall interface due to large difference between the stiffnesses of the wall and soil and due to sliding and separation between the wall and soil. The joint element originally developed by Goodman (1976) can simulates such soil-wall interface behaviors. Referring to Fig. 2.1, the joint element is formulated in the following:

The nodal displacement vector in the s-n local coordinate system is defined as

$$\{u'\}^T = (u_{si}, u_{ni}, u_{sj}, u_{nj}, u_{sk}, u_{nk}, u_{sl}, u_{nl}) \tag{2.157}$$

and also the strain vector as

$$\{\varepsilon\}^T = (\gamma, \varepsilon, \omega) \tag{2.158}$$

where γ, ε and ω are respectively average differential displacements in s and n directions and angular opening between the two sides, expressed by

$$\begin{aligned} \gamma &= \frac{u_{sj} + u_{sl}}{2} - \frac{u_{si} + u_{sk}}{2} \\ \varepsilon &= \frac{u_{nj} + u_{nl}}{2} - \frac{u_{ni} + u_{nk}}{2} \\ \omega &= \frac{u_{nl} - u_{nk}}{L} - \frac{u_{nj} - u_{ni}}{L} \end{aligned} \tag{2.159}$$

The relationship defined in Eq. 2.159 can be rewritten in the matrix form such that

$$\{\varepsilon\} = [L_0]\{u'\} \tag{2.160}$$

where

$$[L_0] = \begin{bmatrix} -\frac{1}{2} & 0 & \frac{1}{2} & 0 & -\frac{1}{2} & 0 & \frac{1}{2} & 0 \\ 0 & -\frac{1}{2} & 0 & \frac{1}{2} & 0 & -\frac{1}{2} & 0 & \frac{1}{2} \\ 0 & \frac{1}{L} & 0 & -\frac{1}{L} & 0 & -\frac{1}{L} & 0 & \frac{1}{L} \end{bmatrix} \tag{2.161}$$

The stress vector in the joint element is defined as

$$\{\sigma\}^T = (\tau_{ns}, \sigma_n, M_0) \tag{2.162}$$

where τ_{ns}, σ_n and M_0 are respectively shear and normal stresses and moment, expressed by

$$\begin{aligned} \tau_{ns} &= \frac{1}{L}(f_{sj} + f_{sl}) \\ \sigma_n &= \frac{1}{L}(f_{nj} + f_{nl}) \\ M_0 &= \frac{L}{2}(f_{nl} - f_{nj}) \end{aligned} \tag{2.163}$$

The nodal force vector is defined as

$$\{f\}^T = (f_{si}, f_{ni}, f_{sj}, f_{nj}, f_{sk}, f_{nk}, f_{sl}, f_{nl}) \tag{2.164}$$

Eqs. 2.163 and 2.164 with $f_{si} = -f_{sj}$ result in

$$\{f\} = [B]\{\sigma\} \tag{2.165}$$

where

$$[B]^T = \begin{bmatrix} -\frac{L}{2} & 0 & 0 \\ 0 & -\frac{L}{2} & \frac{1}{L} \\ \frac{L}{2} & 0 & 0 \\ 0 & \frac{L}{2} & \frac{1}{L} \\ -\frac{L}{2} & 0 & 0 \\ 0 & -\frac{L}{2} & \frac{1}{L} \\ \frac{L}{2} & 0 & 0 \\ 0 & \frac{L}{2} & \frac{1}{L} \end{bmatrix} \tag{2.166}$$

The stress-strain relations at the soil-wall interface are assumed to be as shown in Fig. 2.2. Yield shear stress τ_y is assumed to be

$$\tau_y = \begin{cases} \bar{c} + \sigma_n \tan\bar{\phi} & (\varepsilon \leq 0) \\ 0 & (\varepsilon > 0) \end{cases} \tag{2.167}$$

where $\bar{c}$ and $\bar{\phi}$ = cohesion and friction angle at the soil-wall interface, respectively. Furthermore, the following relationship is assumed:

$$M_0 = \begin{cases} \frac{1}{4}L^3 k_n \omega & (\varepsilon \leq 0) \\ 0 & (\varepsilon > 0) \end{cases} \tag{2.168}$$

With Eqs. 2.160 and 165, the incremental force-displacement relation at the soil-wall interface is obtained as

$$\{df'\} = \{\partial f'\}\left\{\frac{1}{\partial u'}\right\}^T \{du'\} = [B][C][L_0]\{du'\} \tag{2.169}$$

where

$$[C] = \{\partial\sigma\}\left\{\frac{1}{\partial\varepsilon}\right\}^T = \begin{bmatrix} k_s & 0 & 0 \\ 0 & k_n & 0 \\ 0 & 0 & \frac{1}{4}L^3 k_n \end{bmatrix} \tag{2.170}$$

with

$$k_s = \frac{\partial\tau_{ns}}{\partial\gamma}$$
$$k_n = \frac{d\sigma_n}{d\varepsilon} \tag{2.171}$$

Thus the stiffness matrix of the joint element in local coordinates is

$$[K'] = [B][C][L_0] = \frac{L}{4}\begin{bmatrix} [k_a] & [k_b] \\ [k_b] & [k_a] \end{bmatrix} \tag{2.172}$$

with

$$[k_a] = \begin{bmatrix} k_s & 0 & -k_s & 0 \\ 0 & 2k_n & 0 & -2k_n \\ -k_s & 0 & k_s & 0 \\ 0 & -2k_n & 0 & 2k_n \end{bmatrix} \tag{2.173}$$

$$[k_b] = \begin{bmatrix} k_s & 0 & -k_s & 0 \\ 0 & 0 & 0 & 0 \\ -k_s & 0 & k_s & 0 \\ 0 & 0 & 0 & 0 \end{bmatrix} \tag{2.174}$$

The displacement and force vectors in the local coordinate system are expressed by those in the global coordinate system as

$$\{u'\} = [T]\{u\}$$
$$\{f'\} = [T]\{f\} \tag{2.175}$$

where

$$[T] = \begin{bmatrix} [t] & [0] & [0] & [0] \\ [0] & [t] & [0] & [0] \\ [0] & [0] & [t] & [0] \\ [0] & [0] & [0] & [t] \end{bmatrix} \tag{2.176}$$

with

$$[t] = \begin{bmatrix} \cos\alpha & \sin\alpha \\ -\sin\alpha & \cos\alpha \end{bmatrix} \tag{2.177}$$

Then, the tangential stiffness matrix in the global coordinate system can be obtained as

$$[K] = [T]^T[K'][T] \tag{2.178}$$

3. TIME INTEGRATION FOR SOLVING EQUATION

Incremental equation of equilibrium equation for the problem considered is written in the form of

$$[M]\{d\ddot{u}\} + [C]\{d\dot{u}\} + [K]\{du\} = \{df\} \tag{3.1}$$

For the assumed linear variation of the acceleration and the corresponding quadratic and cubic variations of the velocity and displacement, the Taylor expansions at the end of the interval Δt leads to the following equations for increments of velocity and displacement:

$$\{\Delta\dot{u}\} = \{\ddot{u}\}\Delta t + \{\Delta\ddot{u}\}\frac{\Delta t}{2} \tag{3.2}$$

$$\{\Delta u\} = \{\dot{u}\}\Delta t + \{\ddot{u}\}\frac{\Delta t^2}{2} + \{\Delta\ddot{u}\}\frac{\Delta t^2}{6} \tag{3.3}$$

Hence, Eqs. 3.2 and 3.3 result in the incremental displacement and incremental velocity expressed in terms of incremental displacement as follows:

$$\{\Delta\ddot{u}\} = \frac{6}{\Delta t^2}\{\Delta u\} - \frac{6}{\Delta t}\{\dot{u}\} - 3\{\ddot{u}\} \tag{3.4}$$

$$\{\Delta\dot{u}\} = \frac{3}{\Delta t}\{\Delta u\} - 3\{\Delta u\} - 3\{\dot{u}\} - \frac{\Delta\tau}{2}\{\ddot{u}\} \tag{3.5}$$

Introducing Wilson θ method, Eqs. 3.4 and 3.5 result in

$$\{\hat{\Delta}\ddot{u}\} = \frac{6}{\tau^2}\{\hat{\Delta}u\} - \frac{6}{\Delta\tau}\{\dot{u}\} - 3\{\ddot{u}\} \tag{3.6}$$

$$\{\hat{\Delta}\dot{u}\} = \frac{3}{\tau}\{\hat{\Delta}u\} - 3\{\dot{u}\} - \frac{\tau}{2}\{\ddot{u}\} \tag{3.7}$$

where

$$\tau = \theta\,\Delta t \tag{3.8}$$

Substituting Eqs. 3.7 and 3.8 into Eq. 3.1 leads to the following equation of motion:

$$[\hat{K}]\{\hat{\Delta}u\} = \{\hat{\Delta}p\} \tag{3.9}$$

where

$$[\hat{K}] = [K] + \frac{6}{\tau^2}[M] + \frac{3}{\tau}[C] \tag{3.10}$$

$$\{\hat{\Delta}p\} = \{\hat{\Delta}f\} + [M]\left(\frac{6}{\tau}\{\dot{u}\} + 3\{\ddot{u}\}\right) + [C]\left(3\{\dot{u}\} + \frac{\tau}{2}\{\ddot{u}\}\right) \tag{3.11}$$

Solving Eq.3.9 for $\hat{\Delta}u$, the incremental acceleration $\hat{\Delta}\ddot{u}$ is

$$\{\hat{\Delta}\ddot{u}\} = \frac{6}{\tau^2}\{\hat{\Delta}u\} - \frac{6}{\tau}\{\dot{u}\} - 3\{\ddot{u}\} \tag{3.12}$$

and thus

$$\{\Delta\ddot{u}\} = \frac{1}{\theta}\{\hat{\Delta}\ddot{u}\} \tag{3.13}$$

The initial acceleration for next time step is given as

$$\{\ddot{u}\} = [M]^{-1}(\{\Delta f\} - [C]\{\Delta \dot{u}\} - [K]\{\Delta u\}) \qquad (3.14)$$

and the entire process may be repeated for any desired number of time increments to compute the response time history.

4. VERIFICATIONS

4.1 Static Problems

Uniformly distributed vertical load is assumed to be applied on the surface of a saturated homogeneous elastic soil deposits uderlain by impervious base. This corresponds to a classical one dimensional consolidation problem. Theoretical solution for this problem was presented by Terzaghi (1921). For the analysis by the developed program, a soil column, 7ft. high, and 1 ft. wide, is descretized as shown in Fig. 4.1. The material properties are as follows:

Young's modulus (E) = 6000 psf

Poisson's ratio (ν) = 0.4

Coef. of permeability (k) = 2.5×10^{-4} ft/day

Density of water ($\rho_f g$) = 62.5 pcf

The time factor T is defined as

$$T = \frac{c_v t}{H^2} \tag{4.1}$$

where c_v = coefficient of consolidation; t = time; and H = height of the soil column. The coefficient of consolidation cv for the conditions considered in this problem is 5.1428×10^{-2} ft^2/day. Fig. 4.2 shows the variation of the displacements at surface (node A) with time and Fig. 4.3 the variation of excess porewater pressure along the axis of the column at various times.

Good agreements between the finite element results and analytical results can be seen.

A uniform strip load applied on a fluid-saturated homogeneous elasto-porous half space is considered next. This problem has been solved analytically by Schiffman et al. (1969). Finite element descretization of the problem is shown in Fig. 4.4 and the material properties used are

Young's modulus (E) = 1000 KN/m^2
Poison's ratio (v) = 0.
Unit weight of water ($\rho_f g$) = 1000 kg/m^3

The time factor T in this problem is defined as

$$T = \frac{ct}{d^2} \tag{4.2}$$

where d = half of the width of loaded area; and

$$c = \frac{2Gk}{\rho_f} \tag{4.3}$$

with G = shear modulus. Fig. 4.5 shows the computed variation of excess pore pressure, beneath the center of loaded area, at T = 0.1. Good agreements between the finite element results and analytical results can be seen.

4.2 Dynamic Problems

A uniformly distributed vertical load is applied over the surface of a homogeneous fluid-saturated elasto-porous half space. The following two different loading time histories, step function and triangular impulse time histories, are considered as shown in Fig. 4.6. Analytical solutions for those cases were presented by Simon et al. (1984). In the finite element computation, the maximum intensity of the load is 10 units and material properties are as follow:

Young's modulus (E) = 3000 units

Poisson's ratio (ν) = 0.2

Density of fluid (ρ_f) = 0.2977

Density of solid (ρ_s) = 0.3101

Porosity (n) = 0.333

Bulk density (ρ) = 0.306

Coefficient of permeability (k) = 0.004883

Bulk stiffness of solid grain (K_s) = 0.5005×10^4

Bulk stiffness of fluid (K_f) = 0.6106×10^5

The responses are computed for the step loading time history by using the finite element descretization shown in Fig. 4.7 with soil depth = 60 units. The time step (Δt) is 0.002 time units. Figs. 4.8 and 4.9 show respectively the comparisons of the solid and fluid displacements at the surface (node A). Figs. 4.10 and 4.11 show respectively the variations of solid and fluid displacements along the depth at t = 0.06 time units.

The responses are also computed for the triangular impulse loading time history by using the finite element descretization as shown in Fig. 4.7

with soil depth = 120 units. Material properties are same as those aforementioned except $K_s = \infty$ for the present problem. The loading duration (= 2 Δt_0) is 0.021 time units. The time step (Δt) is 0.002 time units. Fig 4. 12 shows the variation of displacement of solid and Fig. 4. 13 shows variation of fluid displacement at surface (node A) with time. Variations of the responses along the depth at t = 0.12 units are also shown in Fig. 4.14 through 4.17 for soild and fluid phases.

5. EXAMPLE OF COMPUTED BEHAVIOR OF WATERFRONT SHEET PILE WALL SUBJECTED TO EARTHQUAKE SHAKING

In 1983, Nihonkai Chubu Earthquake of magnitude 7.7 hit northern part of Japan. The earthquake caused damages to quay walls at the Akita Port located about 100 km from the epicenter. Damages were associated with liquefaction in backfill sand. Fig. 5.1 shows a cross section view of a sheet pile of Oohama No. 2 wharf, at which the water depth is 10 m. This sheet pile was displaced about 1.1 m to 1.8m towards the sea and was cracked due to excessive moment at about 4m above the sea bed. Sand boils and settlements were observed at the apron, indicating liquefaction in backfill induced during the earthquake shaking.

Based on information given by Tsuchida, et al. (1985), the soil at the sheet pile is divided into four homogeneous layers as shown in Fig. 5.1. The properties of each layer are G_{max} = 65030 kpa, max. bulk modulus of soil skeleton = 173400 kpa, $\phi = 37^{o}$, $K_f = 2 \times 10^6$ kpa. The sheet pile is FSP-VI_L type of which second moment of area = 8.6×10^{-4}, cross section area = 0.306 m^2 and density = 7.5 t/m^3. The finite element mesh used is shown in Fig. 5.2. The tie bar is idealized as massless beam elements and hinge connections are assumed at the connections to sheet pile and anchor piles. Two anchor piles and sheet pile are idealized by beam elements. The top ends of two anchor piles are capped with a rigid mass.

Earthquake ground motions, recorded at nonliquefied ground at the Akita Port, were used to determine input motions. The maximum accelerations recorded are 190 gal and 205 gal in the NS and EW

seconds corresponds to the end of shaking. The stress due to the maximum bending computed is 320,000 kpa whereas the failure strength of steel of the sheet pile is 300,000 kpa. Seismic effects significantly increase the earth pressure and bending moment.

REFERENCES

Anzo, Z., 1936, "Dynamic Water Pressure against Retaining Walls during Earthquake," (in Japanese). Proc. 3rd Annual Meeting of Japanese Society of Civil Engineers.

Ayala, G., Romo, M.P., and Gomez, R., 1985,"Earthquake Analysis of Flexible Retaining Walls," Proc. 5th Int. con. Numerical Methods in Geomechanics, Nagoya.

Bolton, M.D. and Steedman, R.S., 1985,"Modelling the Seismic Resistance of Retaining Structures, " Proc. 11th Int. Conf. Soil Mechanics and Foundation Engrg., Vol. 4, pp. 1845-1848.

Clough, G.W. and Duncan, J.M., 1971, "Finite Element Analysis of Retaining Wall Behavior," J. Soil Mechanics and Foundation Engrg., ASCE, Vol.97, SM 12.

Goodman, R.E., Taylor, R.L., and Brekke, T.L., 1968, "A Model for the Mechanics of Jointed Rock," J. Soil Mechanics and Foundation Engrg., Vol. 94, SM3.

Ishibashi, I., Maisuzawa, H., and Kawamura, M., 1985,"Generalized Apparent Seismic Coefficient for Dynamic Lateral Earth Pressure Determination, Proc. 2nd Int. Conf. Soil Dynamics and Earthquake Engineering, Southampton, Vol. 6, pp. 33-42.

Ishii, Y., Arai, H., and Tsuchida, H., 1960, "Material Earth Pressure in an Earthquake," Proc. 2nd World Conf. Earthquake Engrg, Tokyo, Japan.

Jacobsen, L.S., 1939, Described in The Kentucky Project, Technical Report No. 13, Tennessee Valley Authority, 1951.

Kuralowicz, Z. and Tejchman, A., 1984, "Interaction between Flexible Sheet Piling in Cohesionless Soil," Proc. 6th Conf. Soil Mechanics and Foundation Engrg., New Zealand.

Matsuo, H., 1941, "Experimental Study on the Distribution of Earth Pressure Acting on a Vertical Wall during Earthquake Pressure Acting on a Vertical Wall during Earthquake, J. Japanese Society of Civil Engineers, Vol. 27, No. 2.

Matsuo, H. and Ohara, S., 1960, "Lateral Earth Pressure and Stability of Quay Walls during Earthquakes," Proc. 3rd World Conf. Earthquake Engrg., New Zealand.

Matsuo, H. and Ohara, S., 1965, "Dynamic Porewater Pressure Acting on Quay Walls during Earthquakes," Proc. 3rd World Conf. Earthquake Engineering, New Zealand.

The Minister of Transportation, 1964, "Damages of Ports and Harbors Caused by the Niigata Earthquake," (Japanese).

Mononobe, N., 1929, "Earthquake-Proof Construction of Masnary Dams," Proc. World Engineering Conf., Vol. 9, p. 275.

Mononobe, N. and Matsuo, H., 1929, "On the Determination of Earth Pressure during Earthquakes," Proc. Engineering Conf., Vol. 9, p. 176.

Murphy, V.A., 1960, "The Effect of Ground Characteristics on the Aseismic Design of Structures," Proc. 2nd World Conf. Earthquake Engrg., Vol. 1, pp. 231-247.

Okabe, S., 1926, "General Theory of Earth Pressure," J. Japanese Society of Civil Engineers, Vol. 12, No. 1.

Potts, D.M. and Fourie, A.B., 1986, A Numerical Study of the Effects of Wall Deformation on Earth Pressures. Int. J. Numerical and Analytical Methods in Geomechanics, Vol. 10, pp. 383-405.

Prakash, S. and Basavanna, B.M., 1969, "Earth Pressure Distribution Behind Retaining Walls during Earthquake," Proc. 4th World Conf Earthquake Engrg., Santiago, Chile.

Saabzevari, A. and Ghaahramani, A., 1974, "Dynamic Passive Earth Pressure Problem, J. Geotechnical Engrg., ASCE, Vol. 100, GT1, pp. 15-30.

Schifman, R.L., Chen, A.T. and Jordan, J.C., 1969, "An Analysis of Consolidation Theories," Int. J. Soil Mechanics and Foundation Engineering, ASCE, Vol. 95, pp. 285-312.

Seed, H.B. and Whitman, R.V., 1970, "Design of Earth Retaining Structures for Dynamic Loads," Lateral Stresses in the Ground and Design of Earth-Retaining Structures, ASCE.

Simon, B.R., Zienkiewicz, O.C. and Paul, D.K., 1984, "An Analytical Solution for Transient Response of Saturated Porous Elastic Solid, Int. J. Numerical and Analytical Methods in Geomechanics, Vol. 8, pp. 381-398.

Tajimi, H. 1973, "Dynamic Earth Pressure on Basement Wall," Proc. 5th World Conf. Earthquake Engrg., Rome, Italy.

Terzaghi, K., 1925, "Principle of Soil Mechanics," Engrg. News Record.

Towhata, I. and Islam, S., 1987, "Prediction of Lateral Displacement of Anchored Bulkheads Induced by Seismic Liquefaction," J. Soils and Foundation, Vol. 27, No.4, pp.137-147.

Tsuchida, H. et al., 1985, "Damage to Port Structures by the 1983 Nipponkai-Chubu Earthquake," Technical Note of the Port and Harbor Research Institute, No. 511, p. 447

Zienkeiewicz, O.C. and Shiomi, T., 1984, "Dynamic Behavior of Saturated Porous Media; The Generalized Biot Formulation and Its Numerical Solution," Int. J. Numerical and Analytical Methods in Geomechanics, Vol. 8, pp. 71-96.

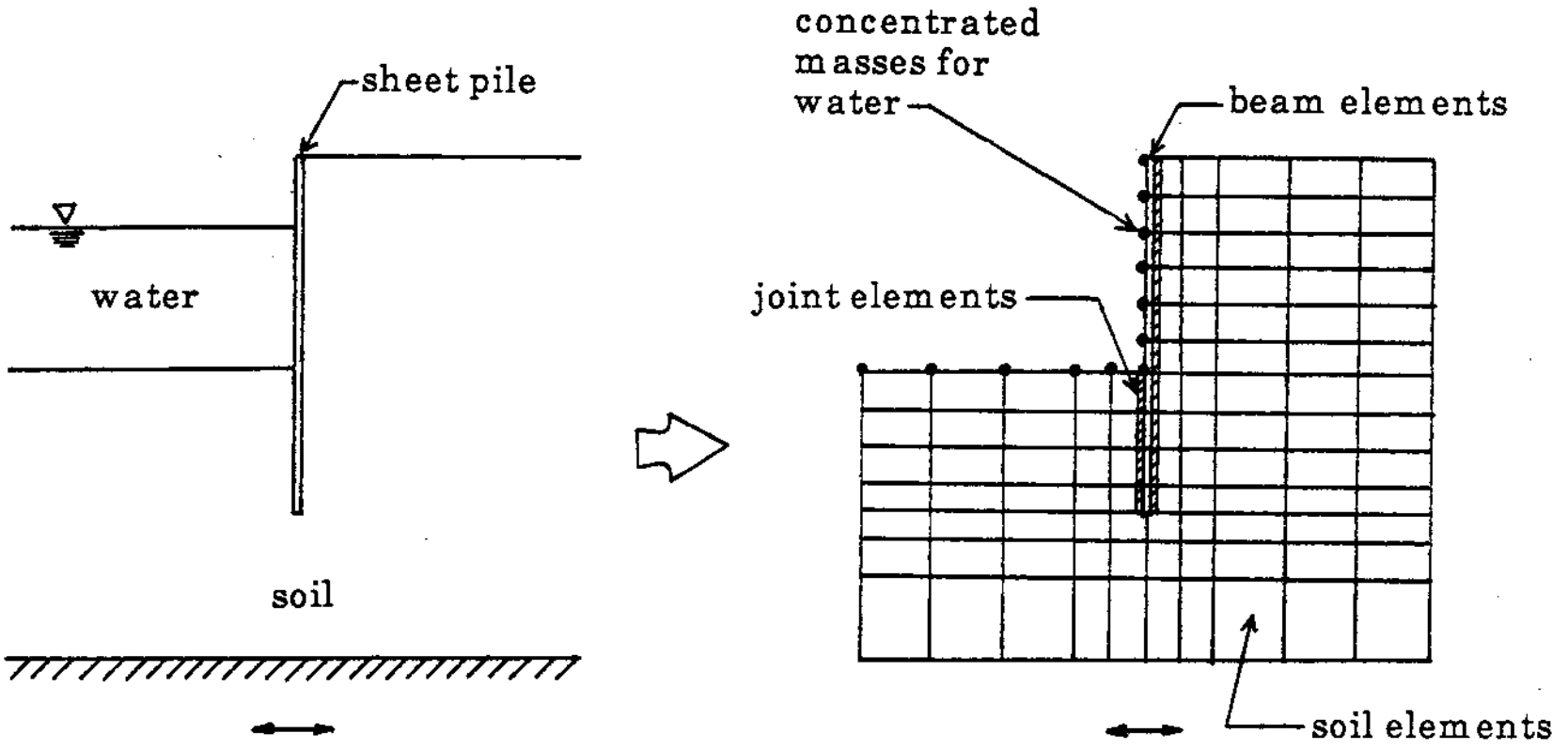

Fig. 1.1 Finite Element Model of a Waterfront Sheet Pile Wall

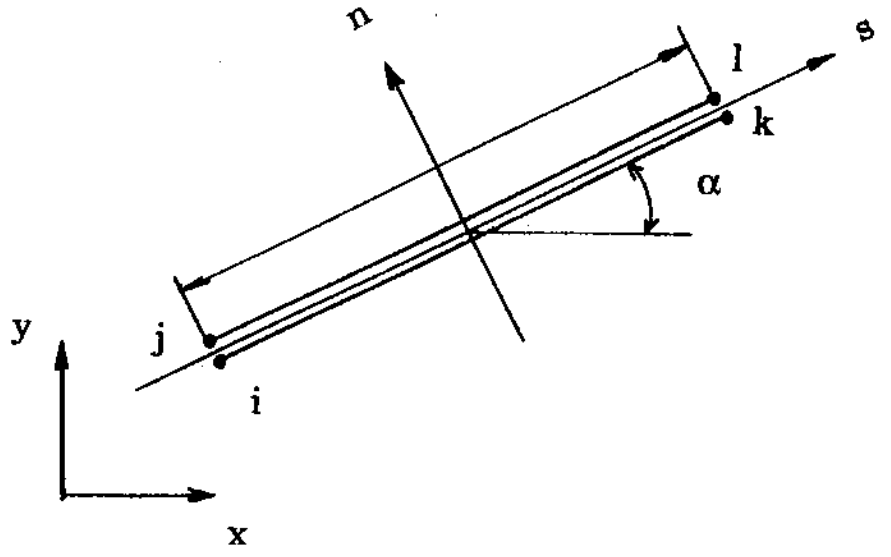

Fig. 2.1 Joint Element

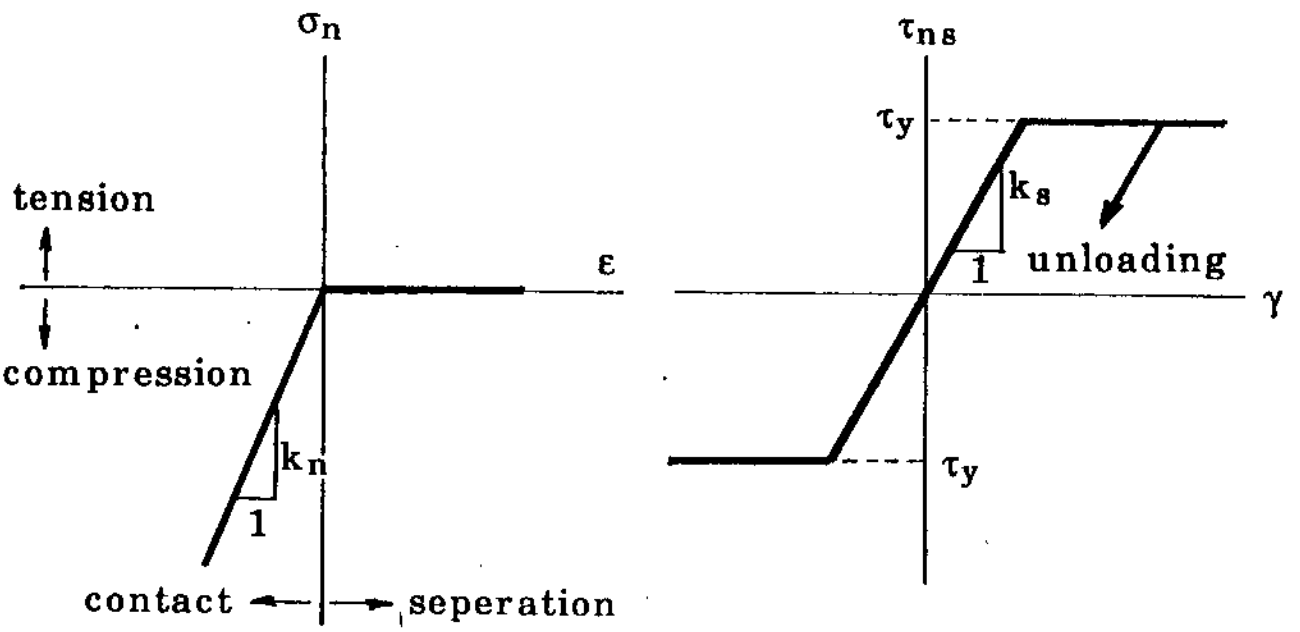

Fig. 2.2 Stress-Strain Relationship at Soil-Wall Interface

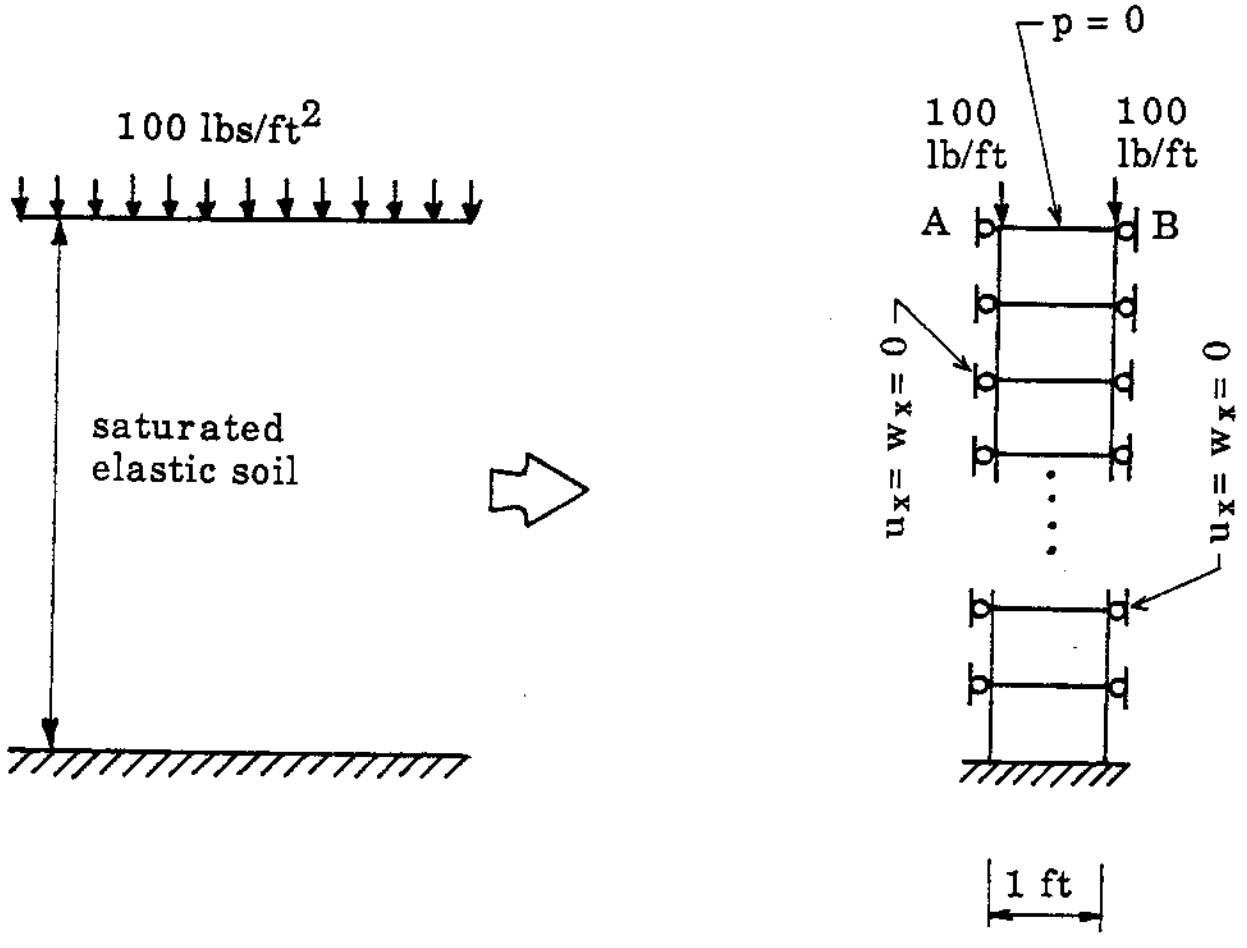

Fig. 4.1 Conditions and Finite Element Model Used for Verification Study
(Static 1-D Problem)

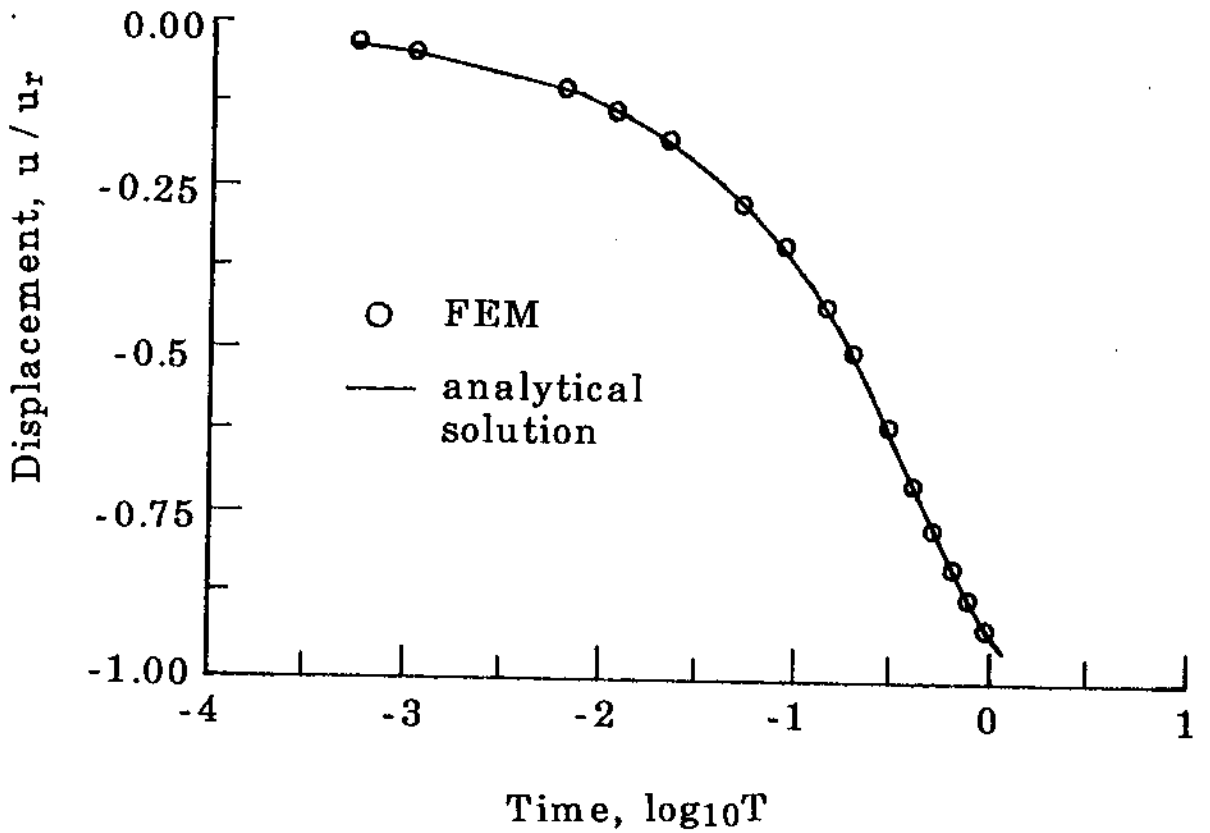

Fig. 4.2 Time-Settlement Curve

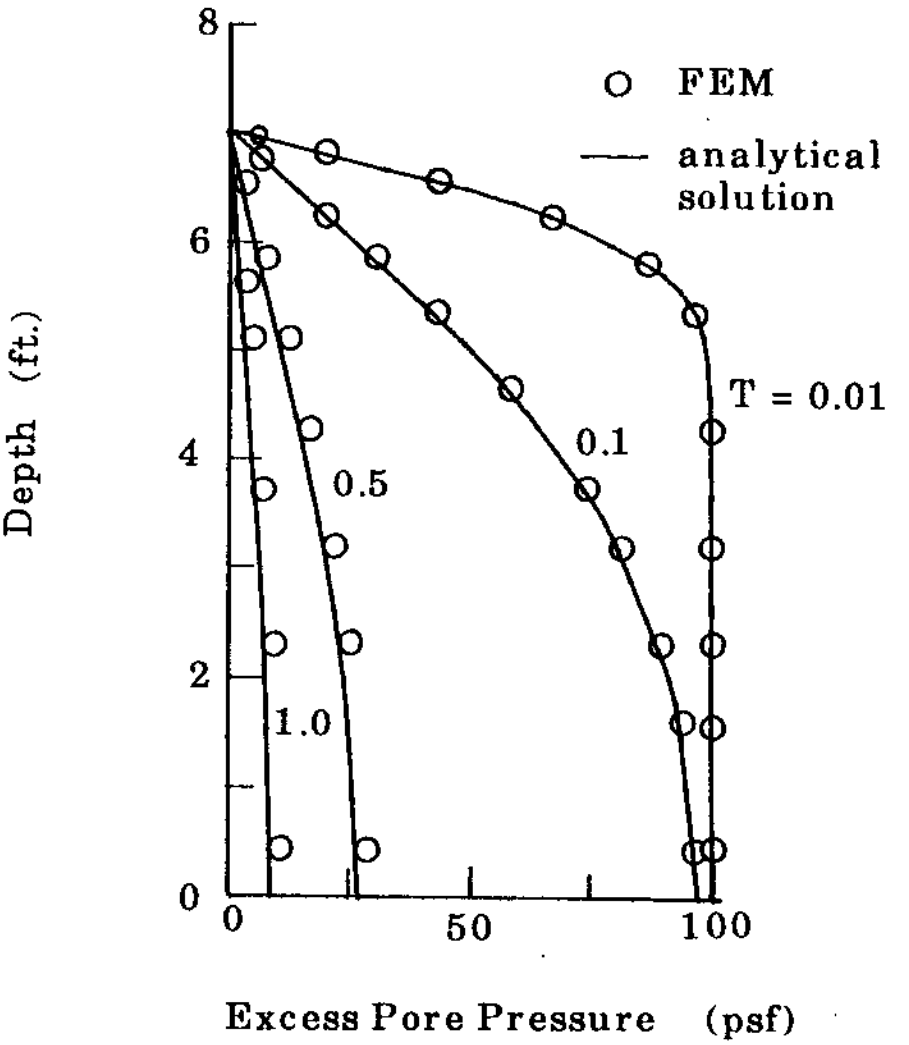

Fig. 4.3 Variations of Excess Pore Pressure with Depth at Various Times (Static 1-D problem)

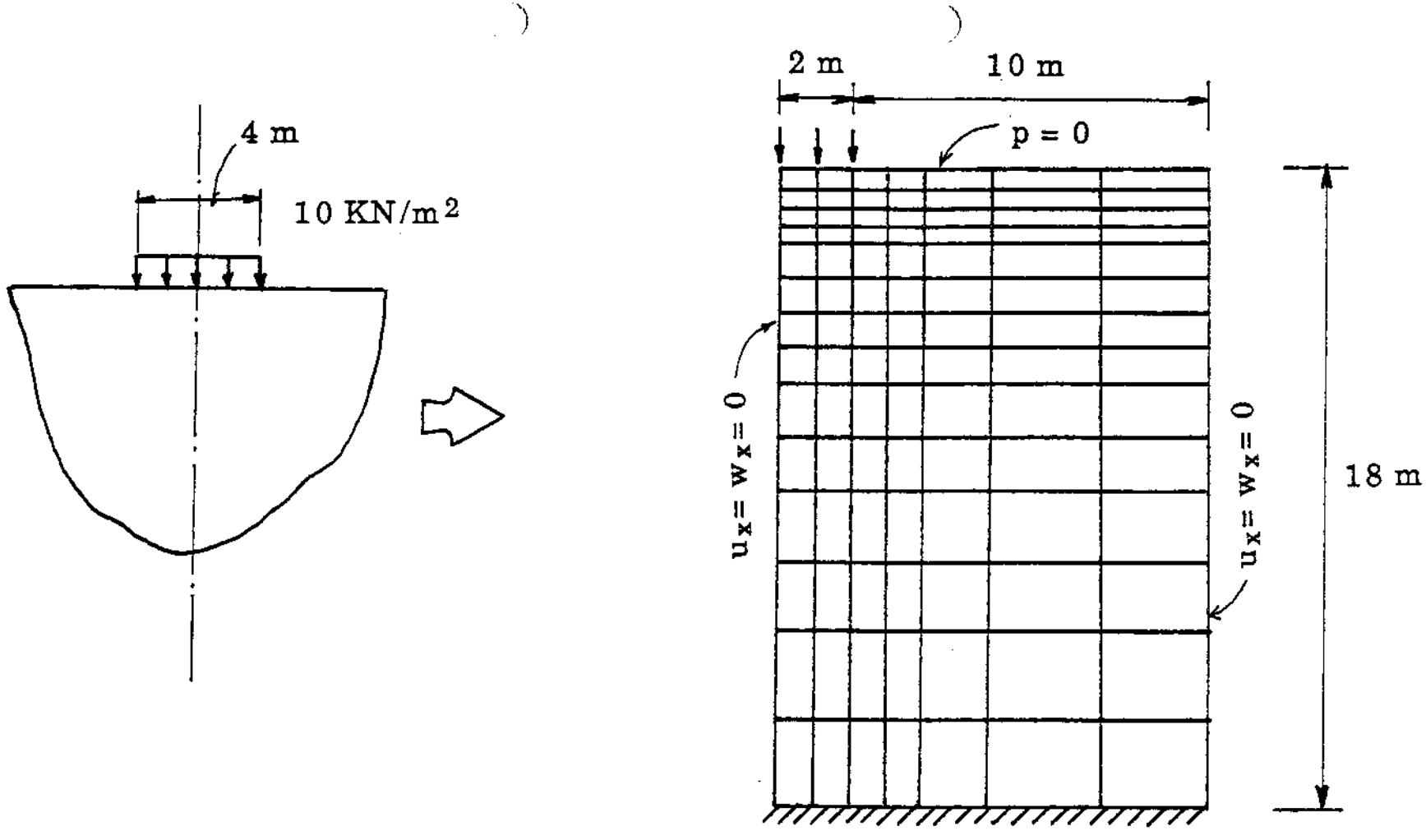

Fig. 4.4 Conditions and Finite Element Model Used for Verification Study
(Static 2-D Problem)

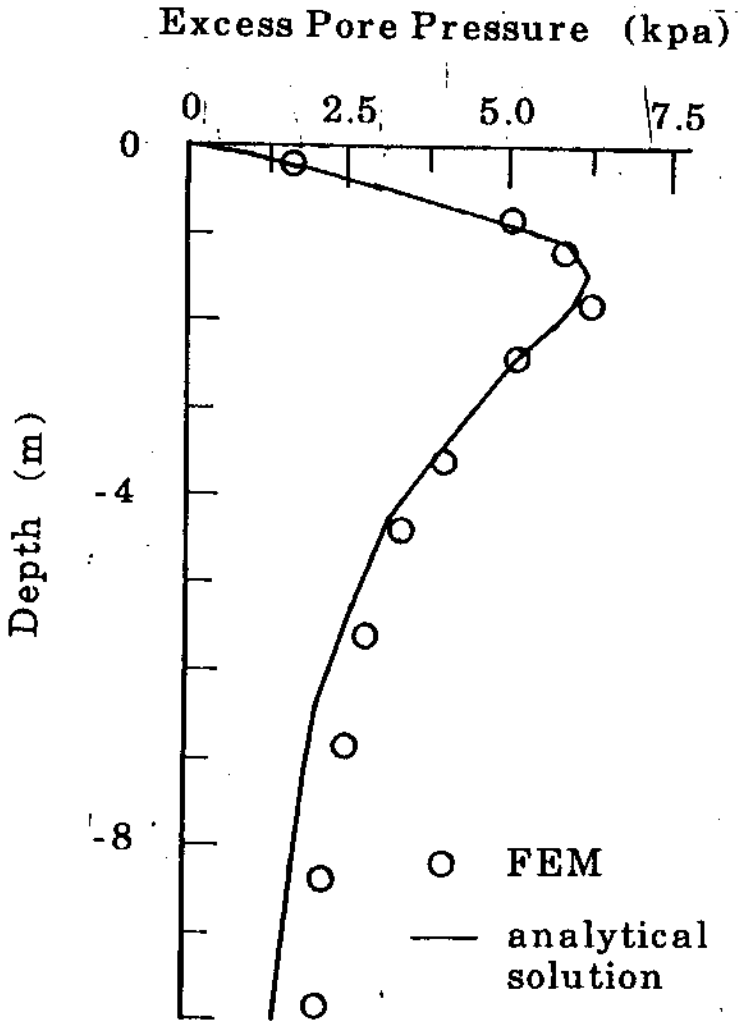

Fig. 4.5 Variation of Excess Pore Pressure with Depth beneath the Loaded Area at T = 0.1

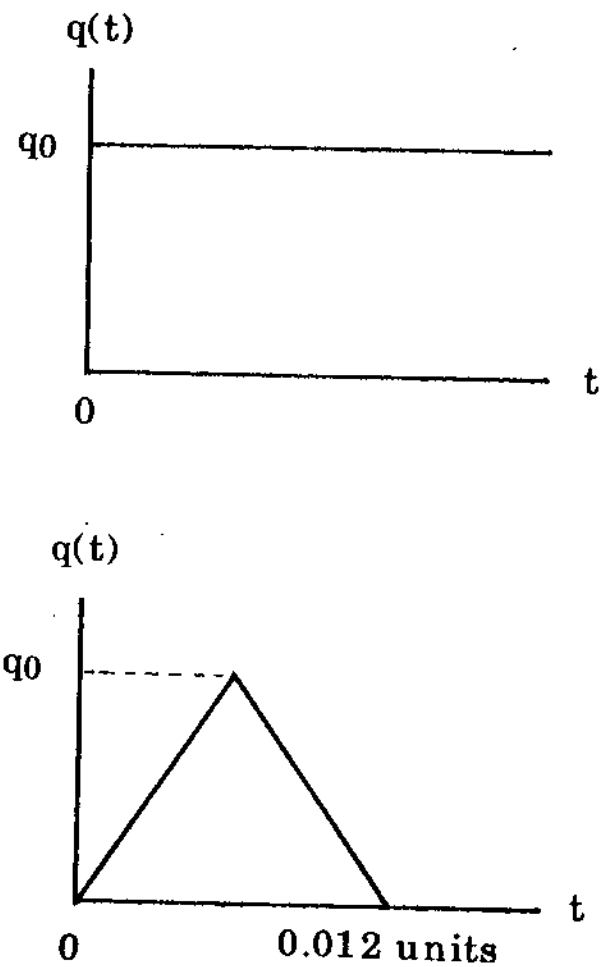

Fig. 4.6 Loading Time Histories

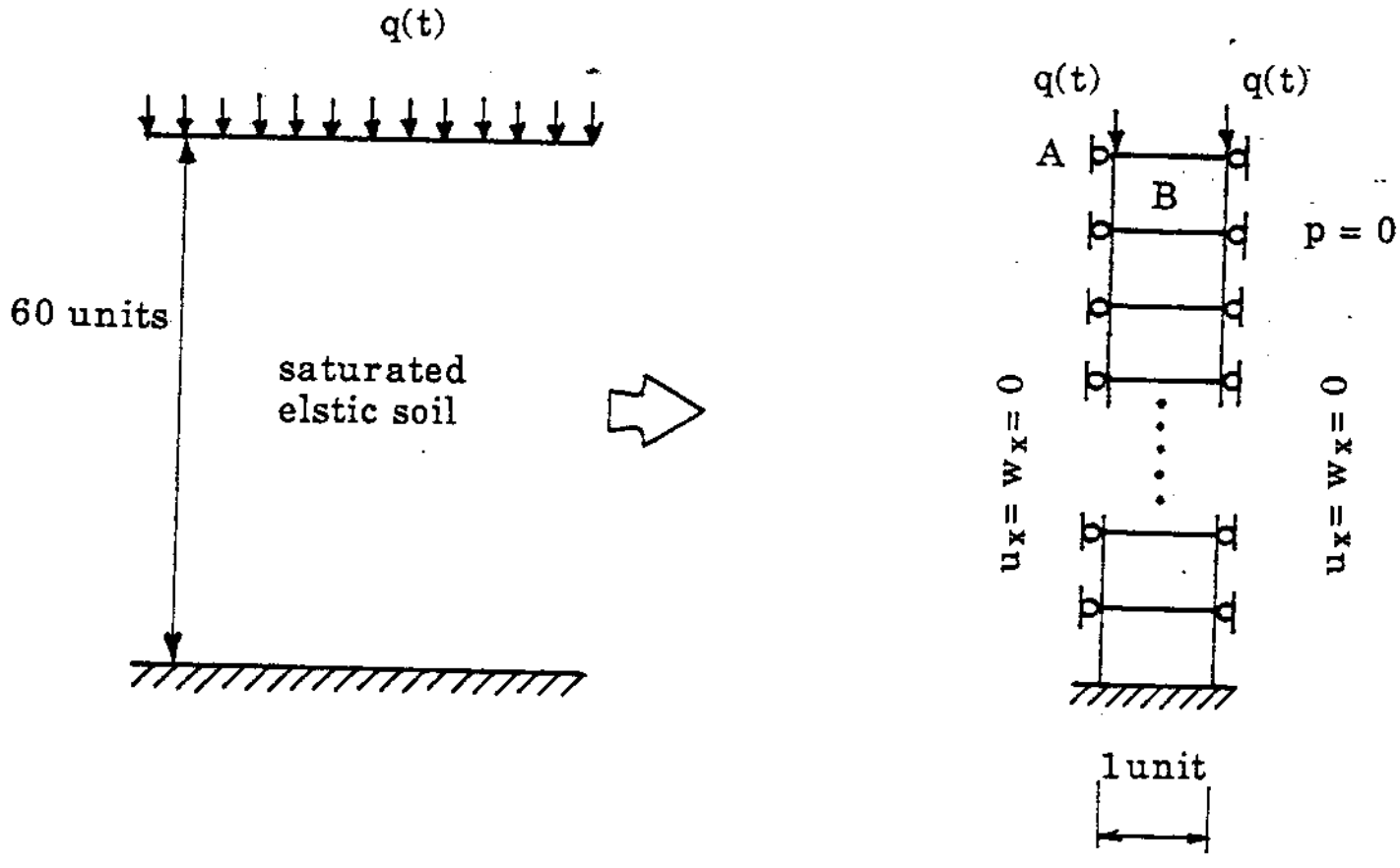

Fig. 4.7 Conditions and Finite Element Model Used for Verification Study
(Dynamic 1-D Problem)

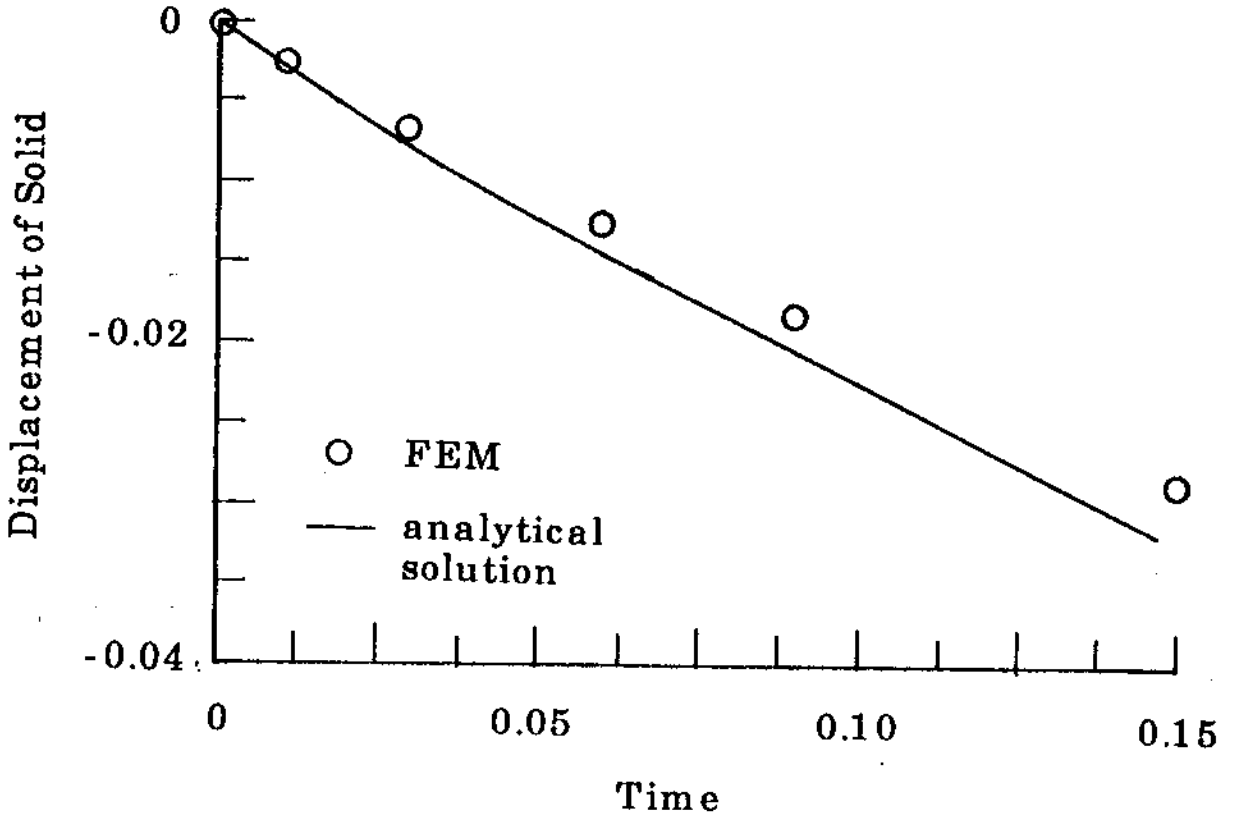

Fig. 4.8 Variation of Displacement of Solid at Surface with Time (Step Function Loading)

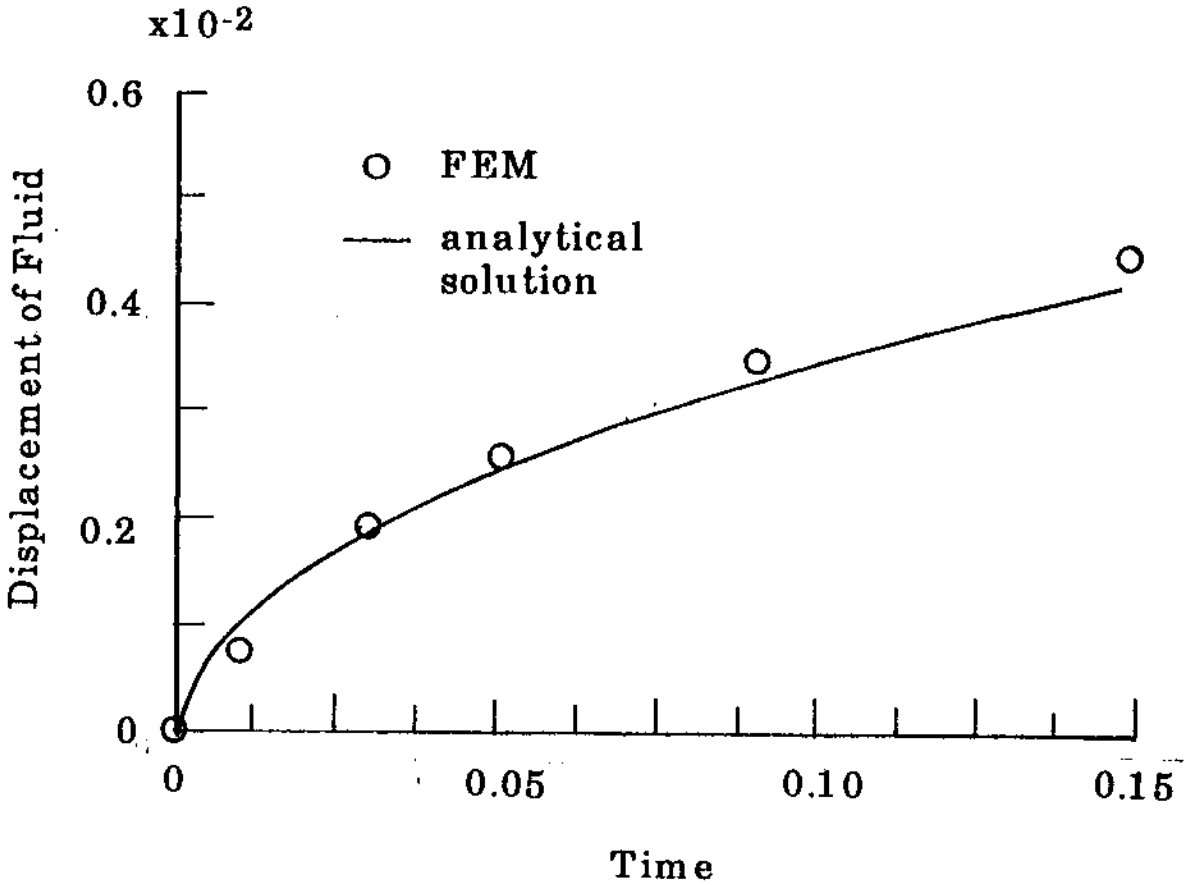

Fig. 4.9 Variation of Displacement of Fluid at Surface with Time (Step Function Loading)

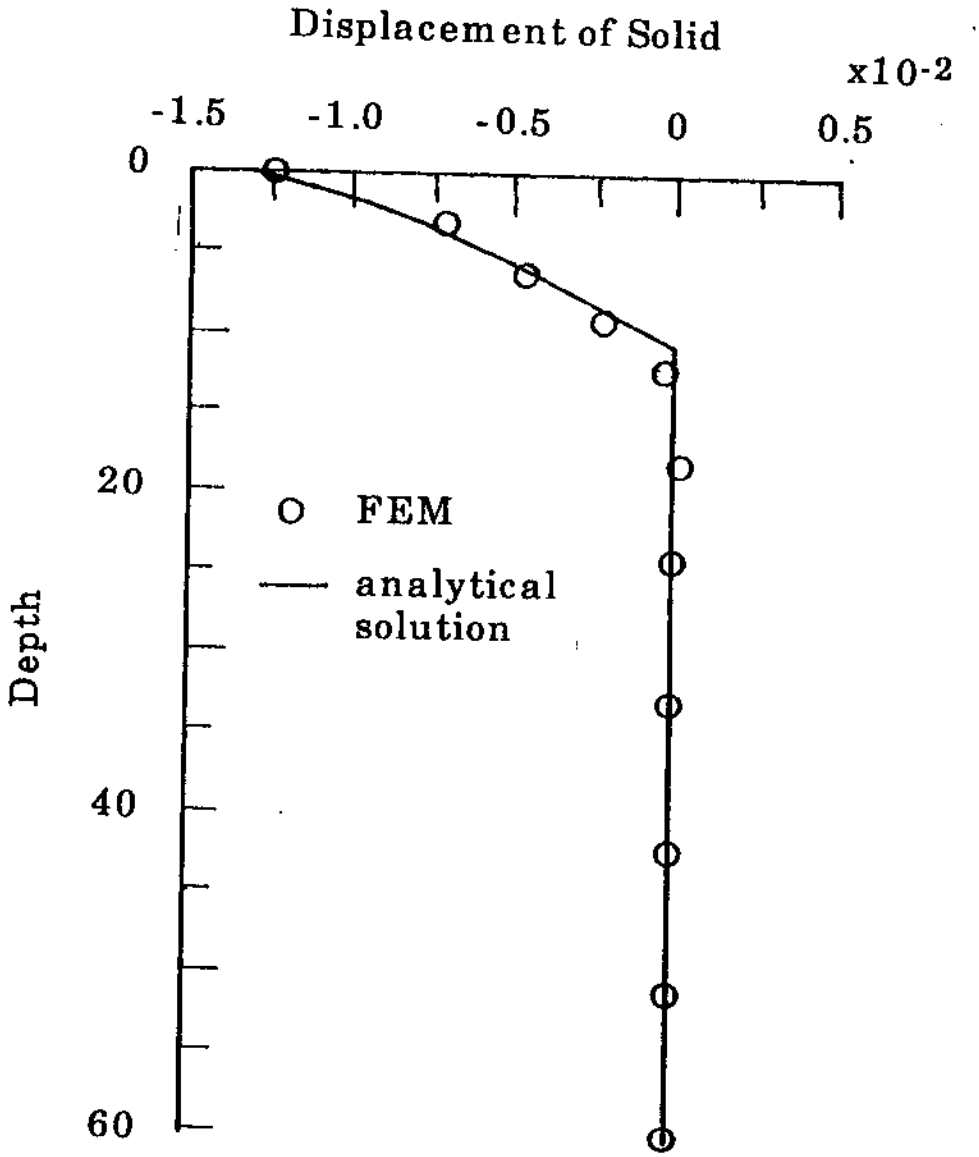

Fig. 4.10 Variation of Displacement of Solid with depth at t = 0.06 (Step Function Loading)

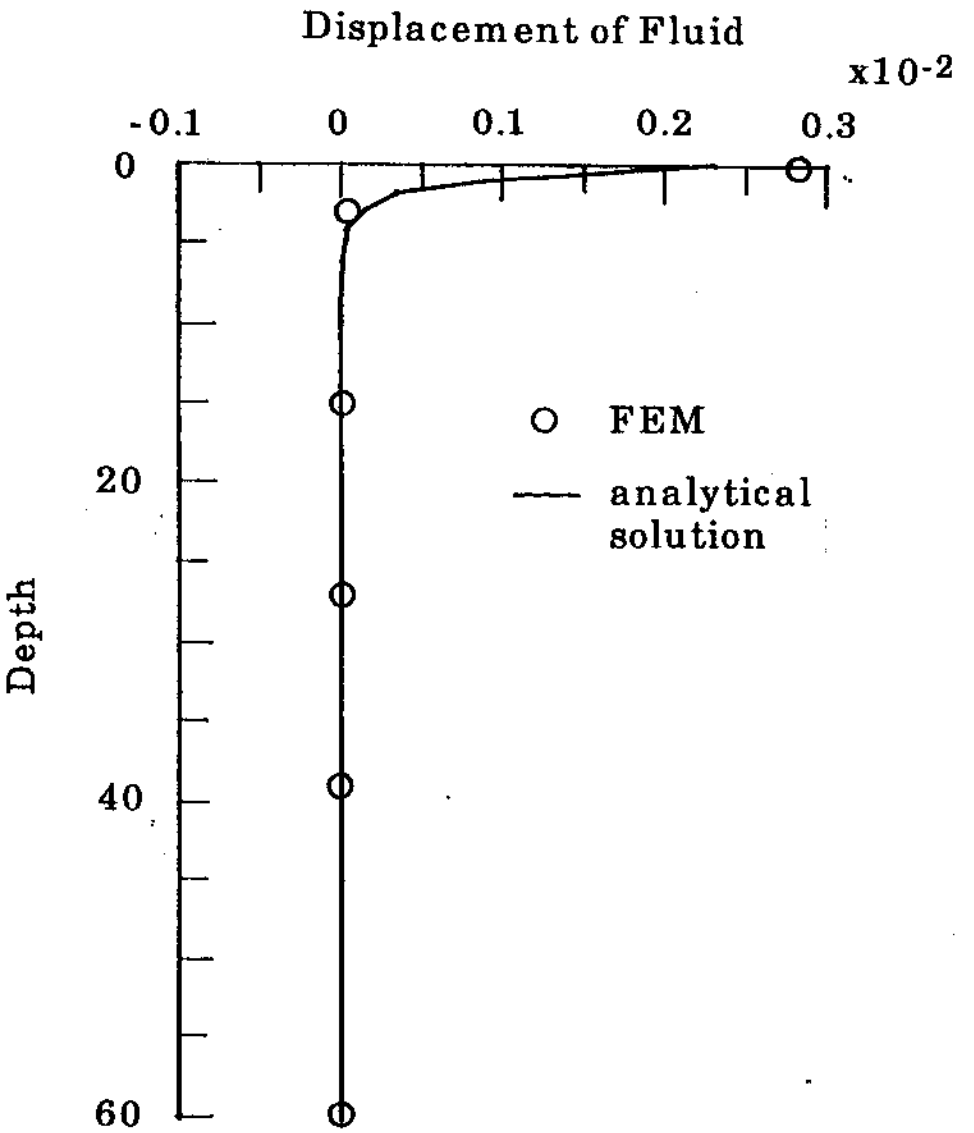

Fig. 4.11 Variation of Displacement of Fluid with Depth at t = 0.06 (Step Function Loading)

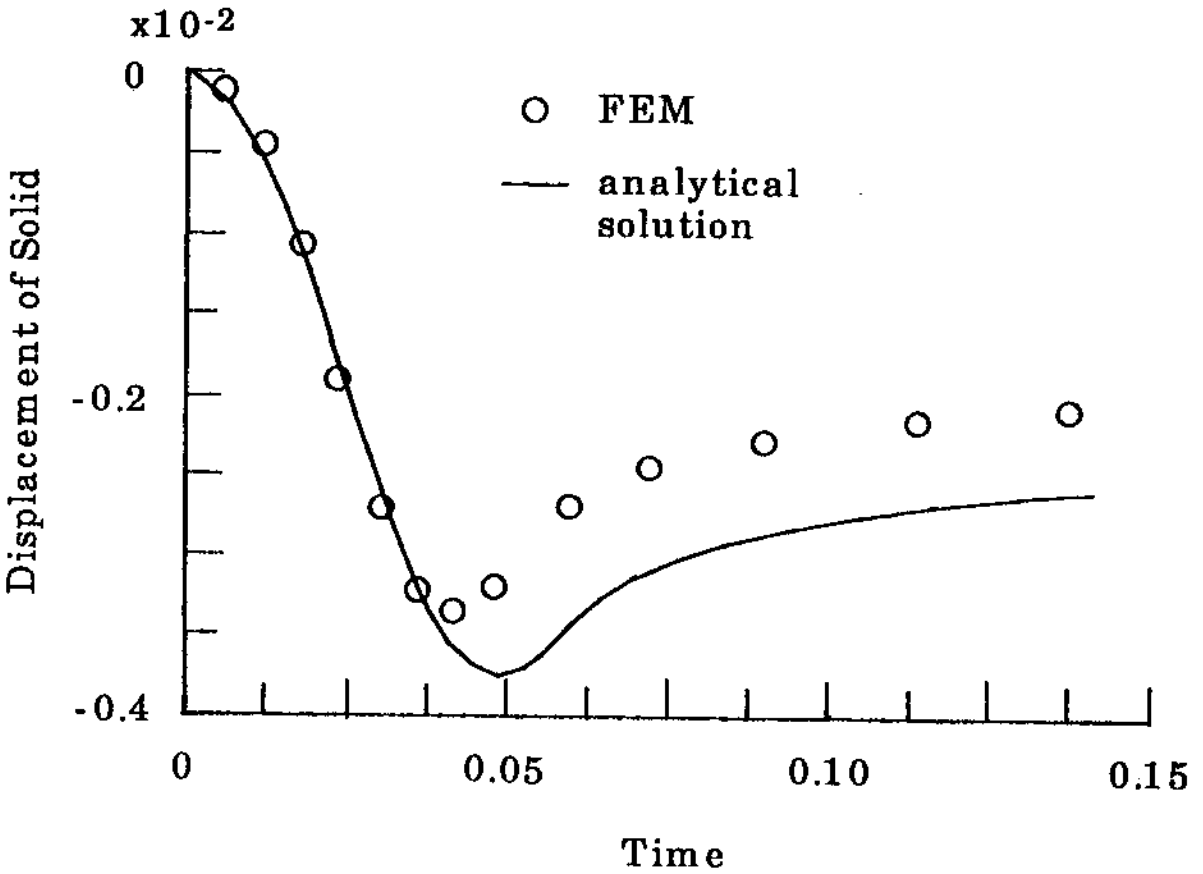

Fig. 4.12 Variation of Displacement of Solid at Surface with Time (Triangular Impulse Loading)

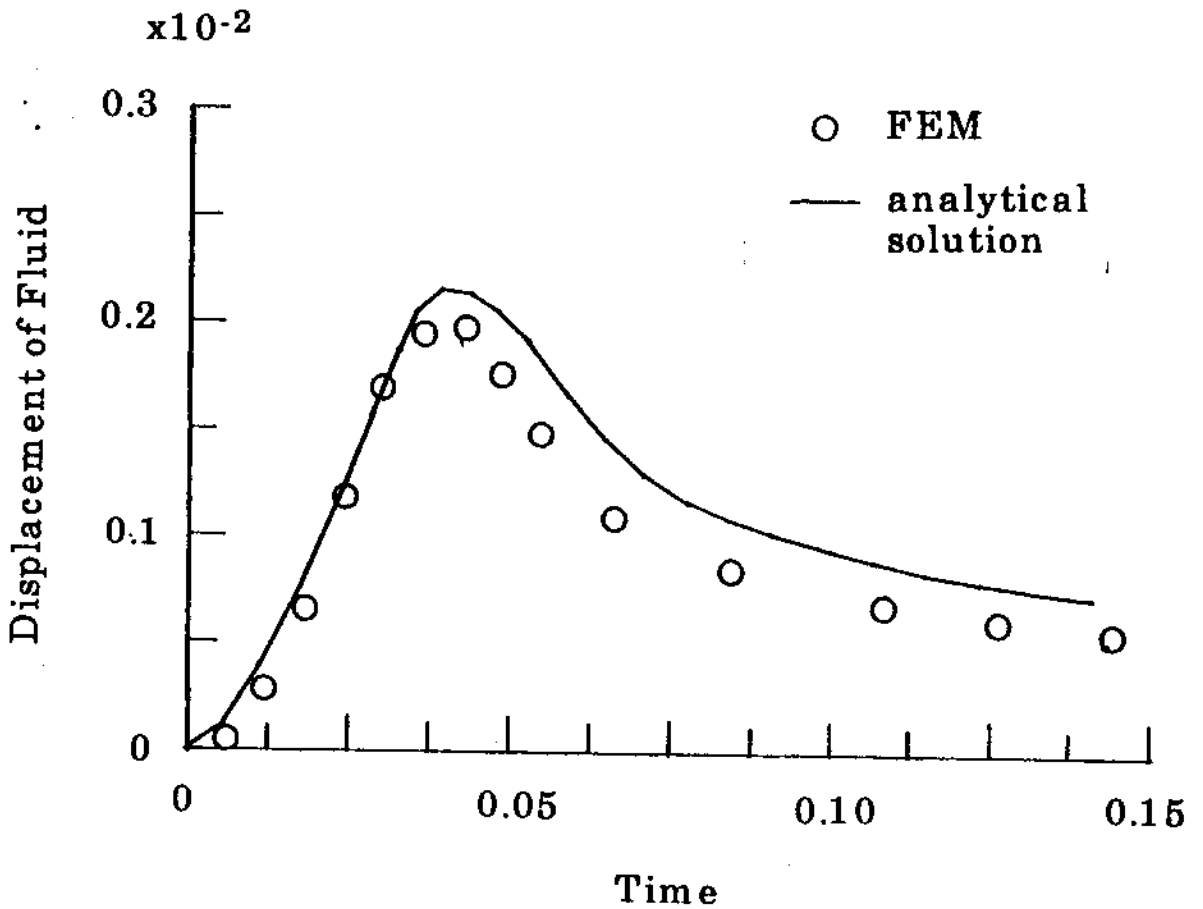

Fig. 4.13 Variation of Displacement of Fluid at Surface with Time (Triangular Impulse Loading)

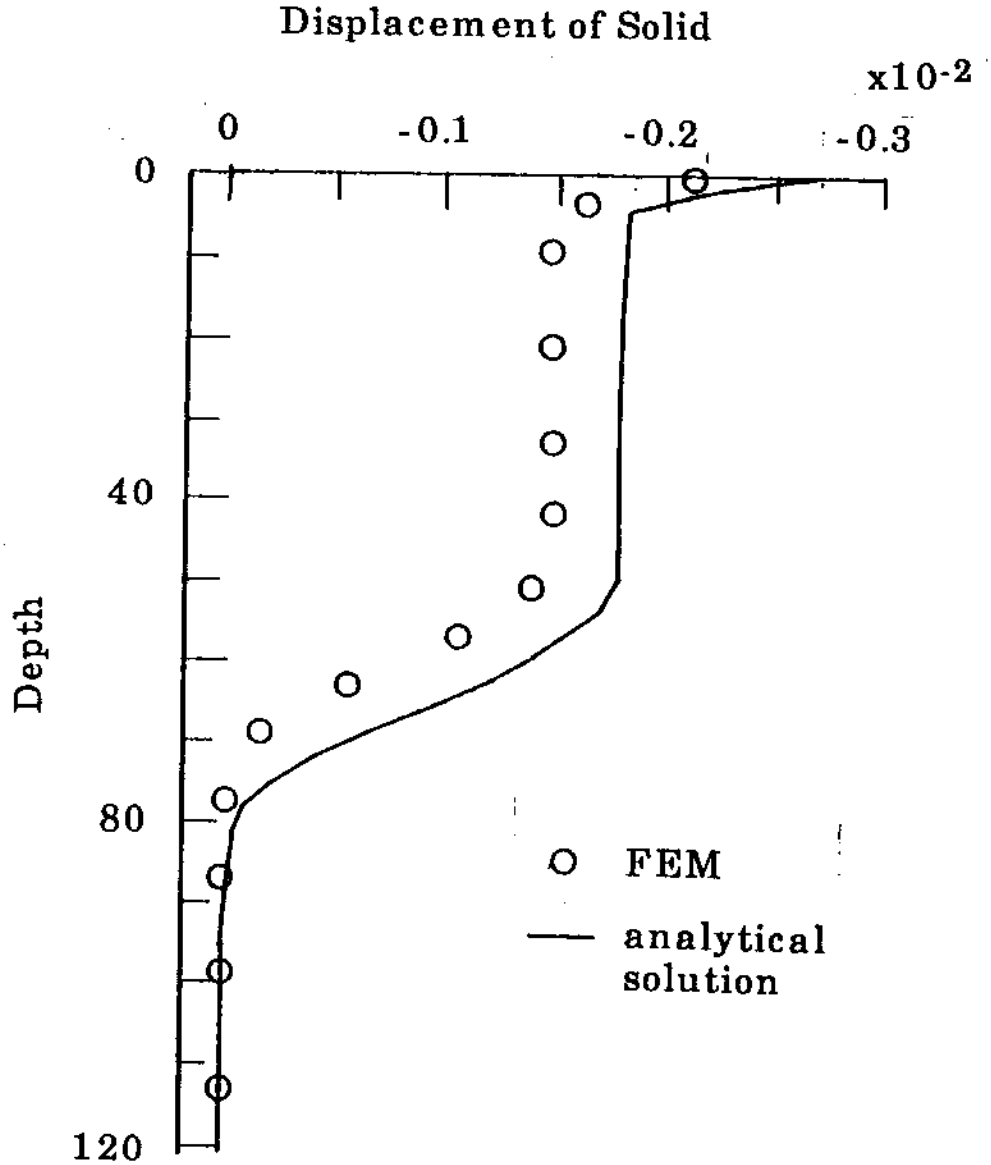

Fig. 4. 14 Variation of Displacement of Solid with Depth at t = 0.12
(Triangular Impulse Loading)

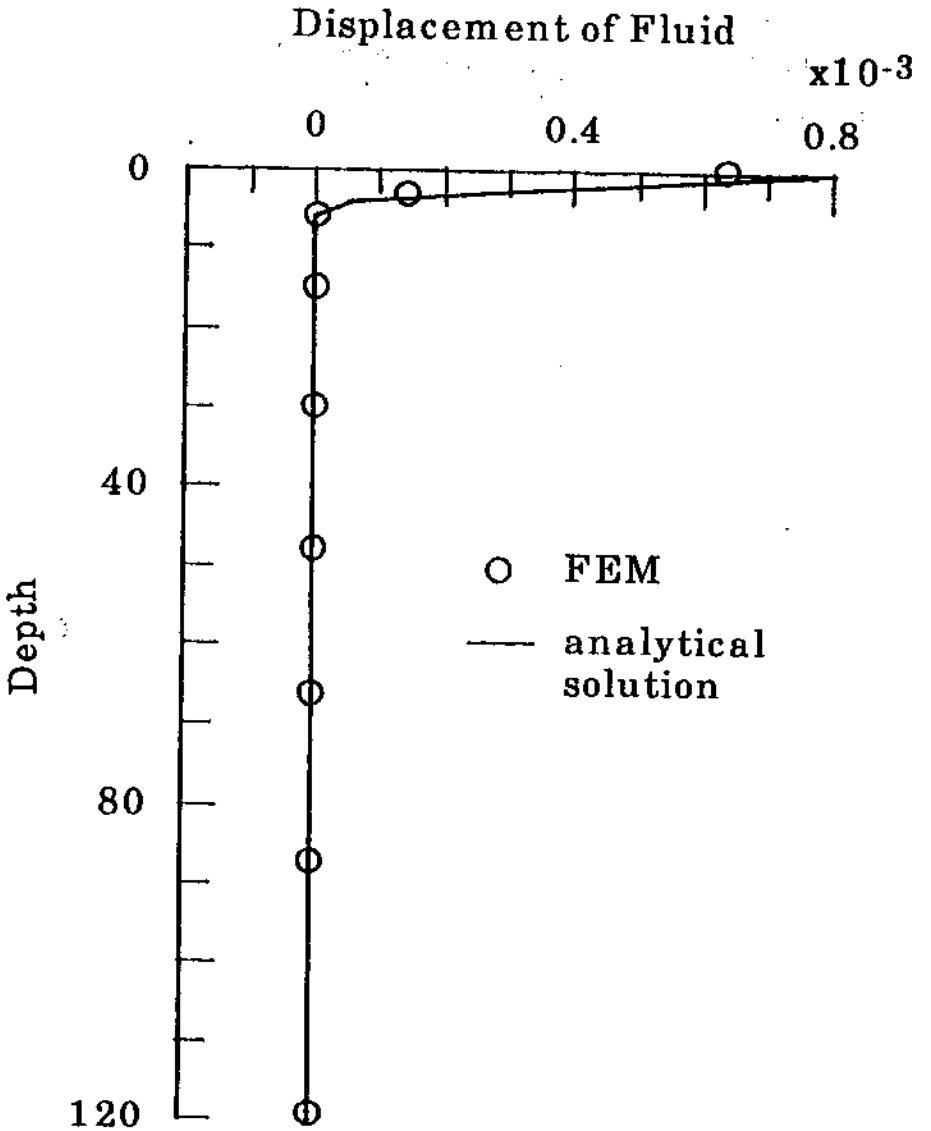

Fig. 4.15 Variation of Displacement of Fluid with Depth at t = 0.12
(Triangular Impulse Loading)

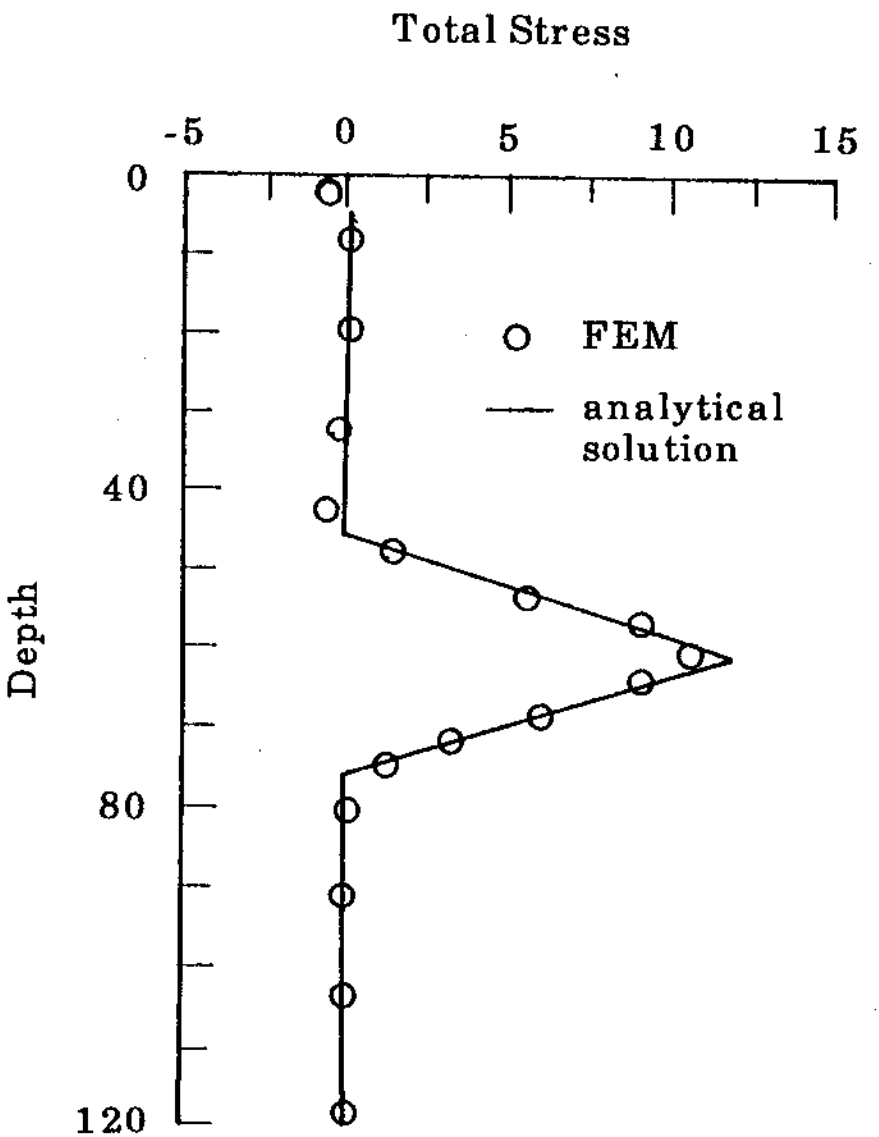

Fig. 4.16 Variation of Total Stress with Depth at t = 0.12
(Triangular Impulse Loading)

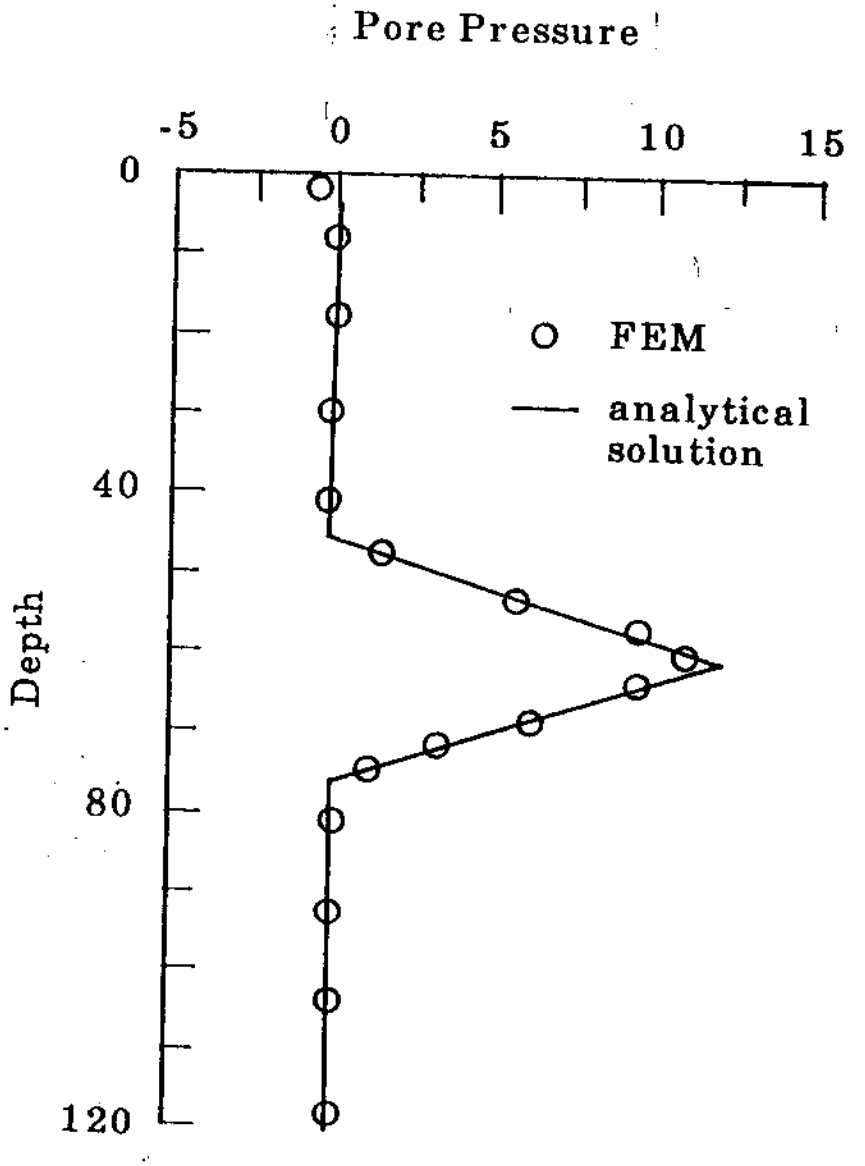

Fig. 4.17 Variation of Excess Pore Pressure with Depth at $t = 0.12$ (Triangular Impulse Loading)

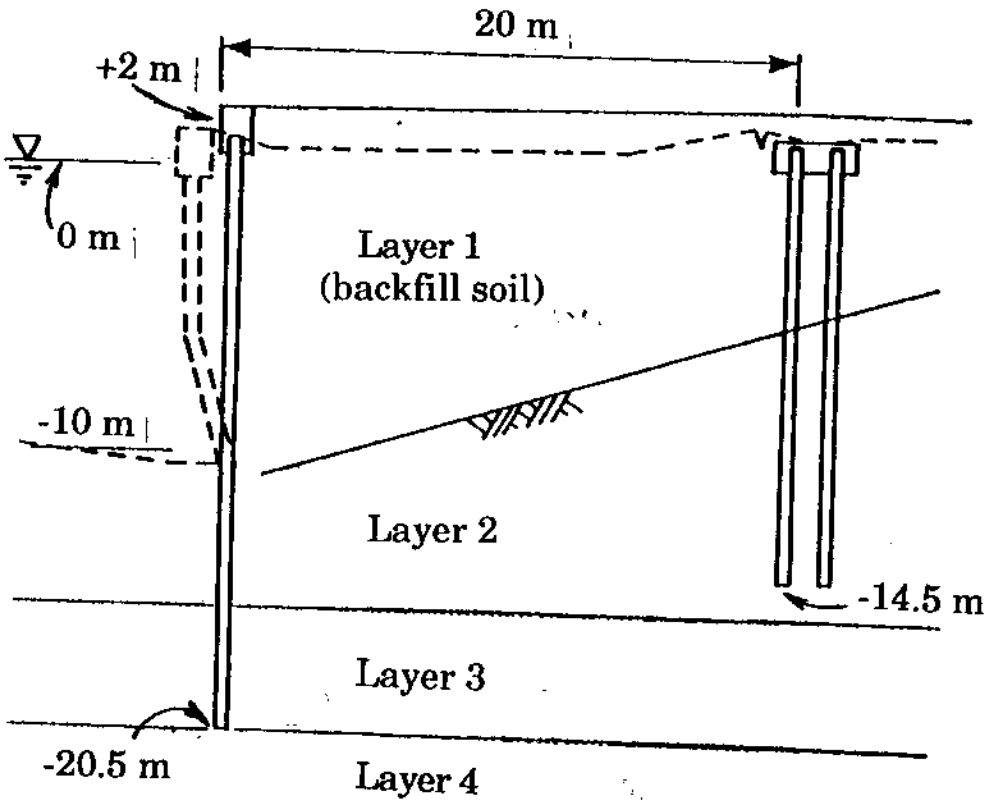

Fig. 5.1 Anchored Bulkhead of Oohama No. 2 Wharf

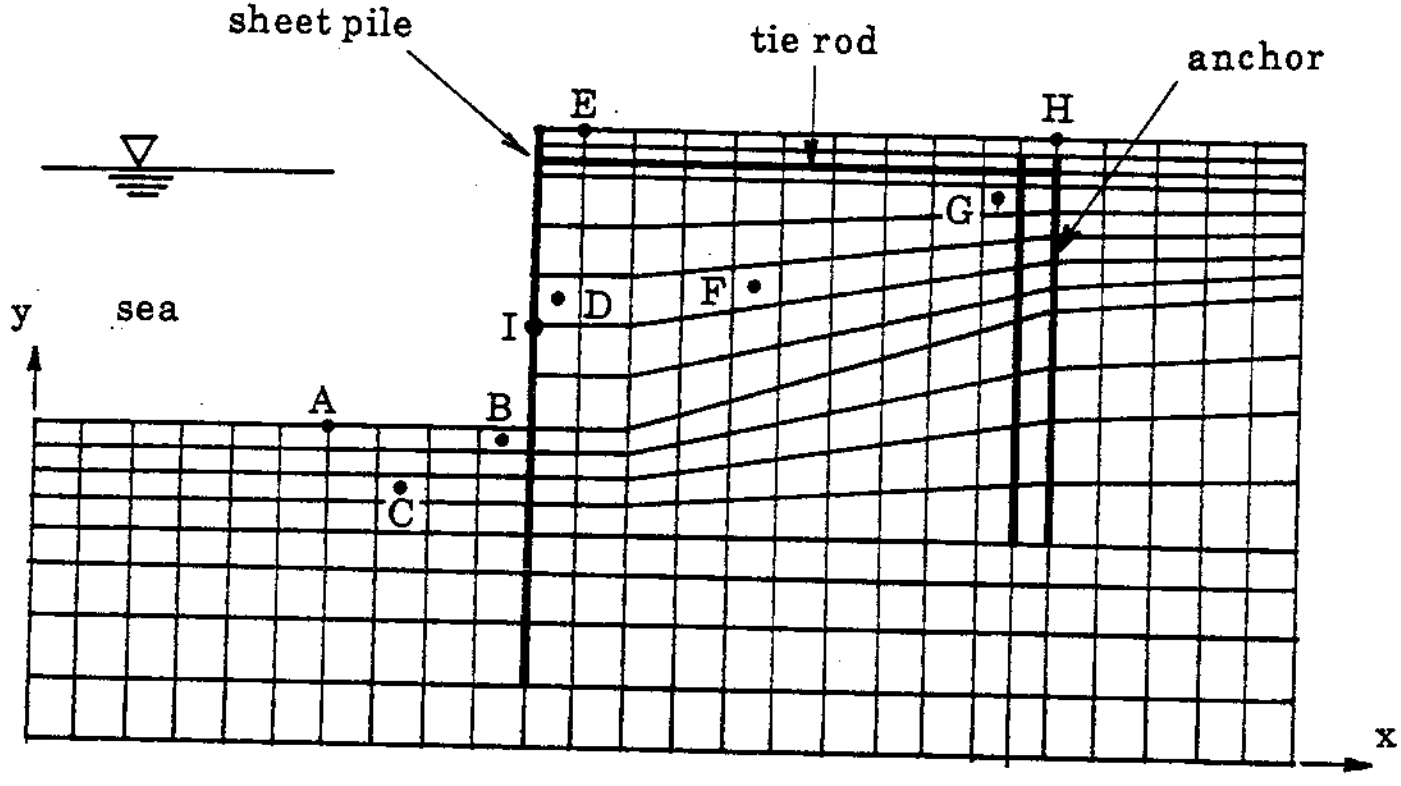

Fig. 5.2 Finite Element Descretization Used in Analysis

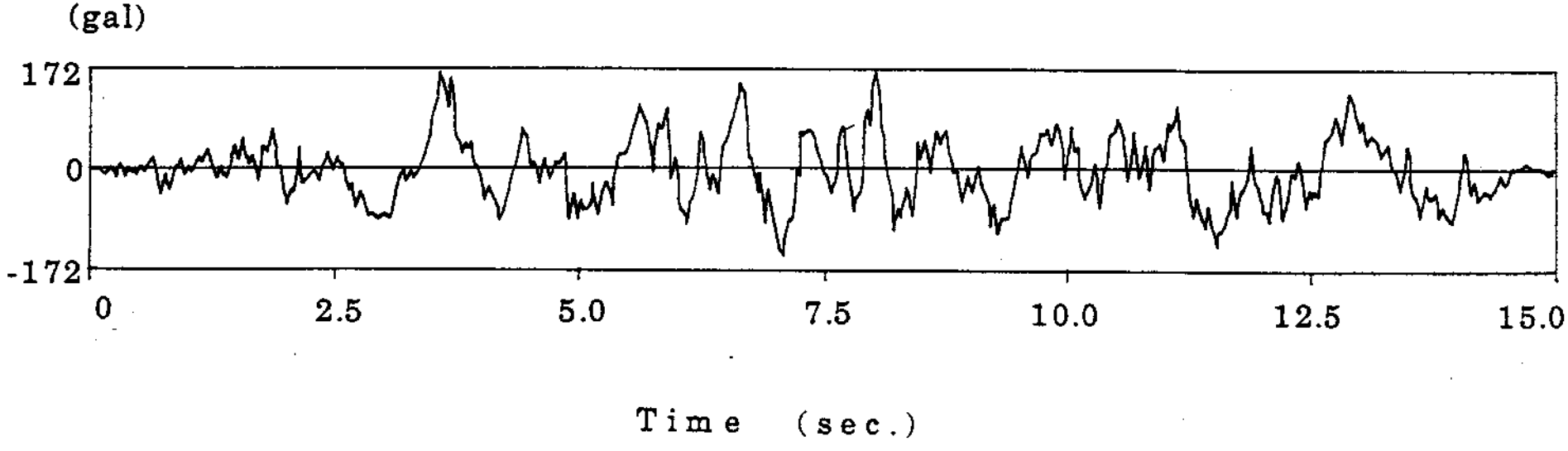

Fig. 5.3 Computed Input Bedrock Acceleration Time History

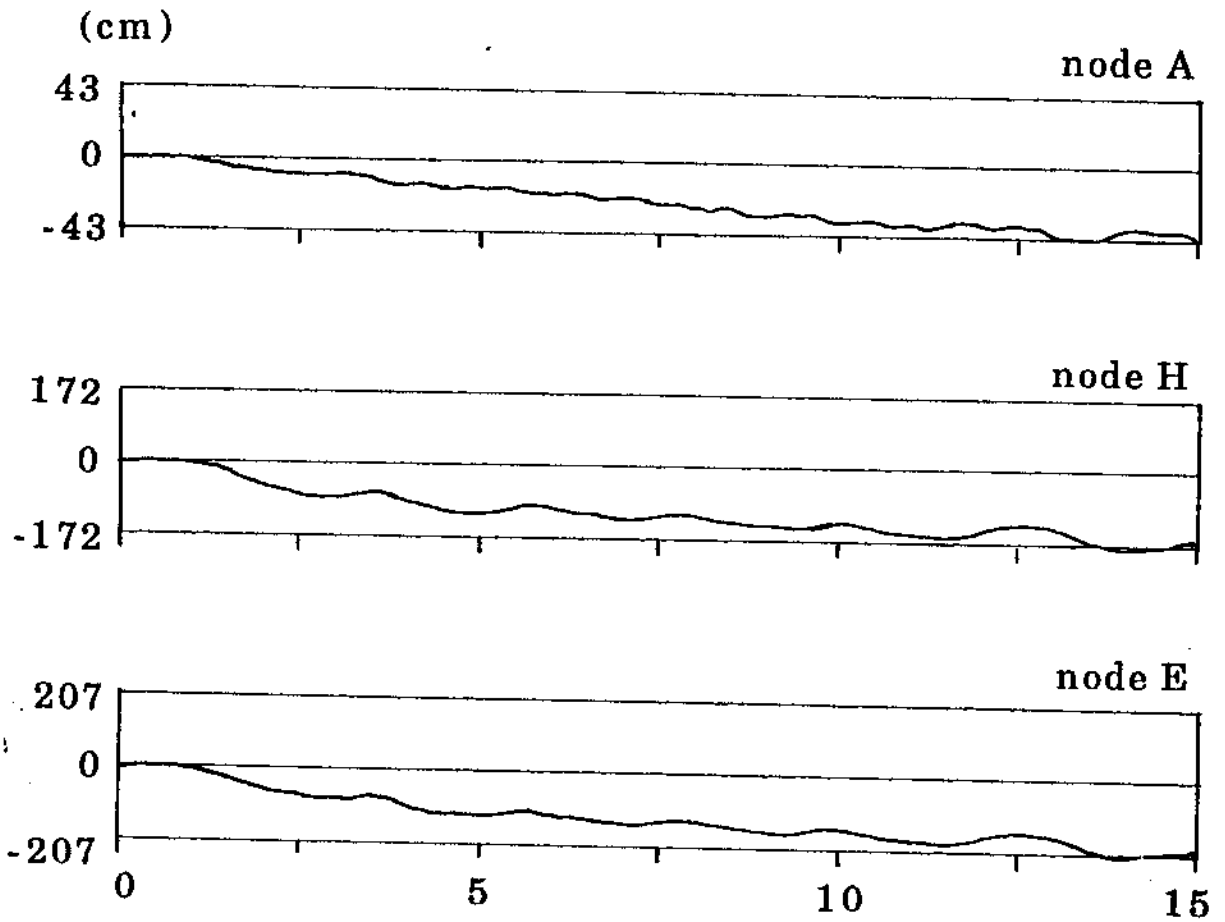

Fig. 5.4 Horizontal Displacement Time Histories at Various Locations

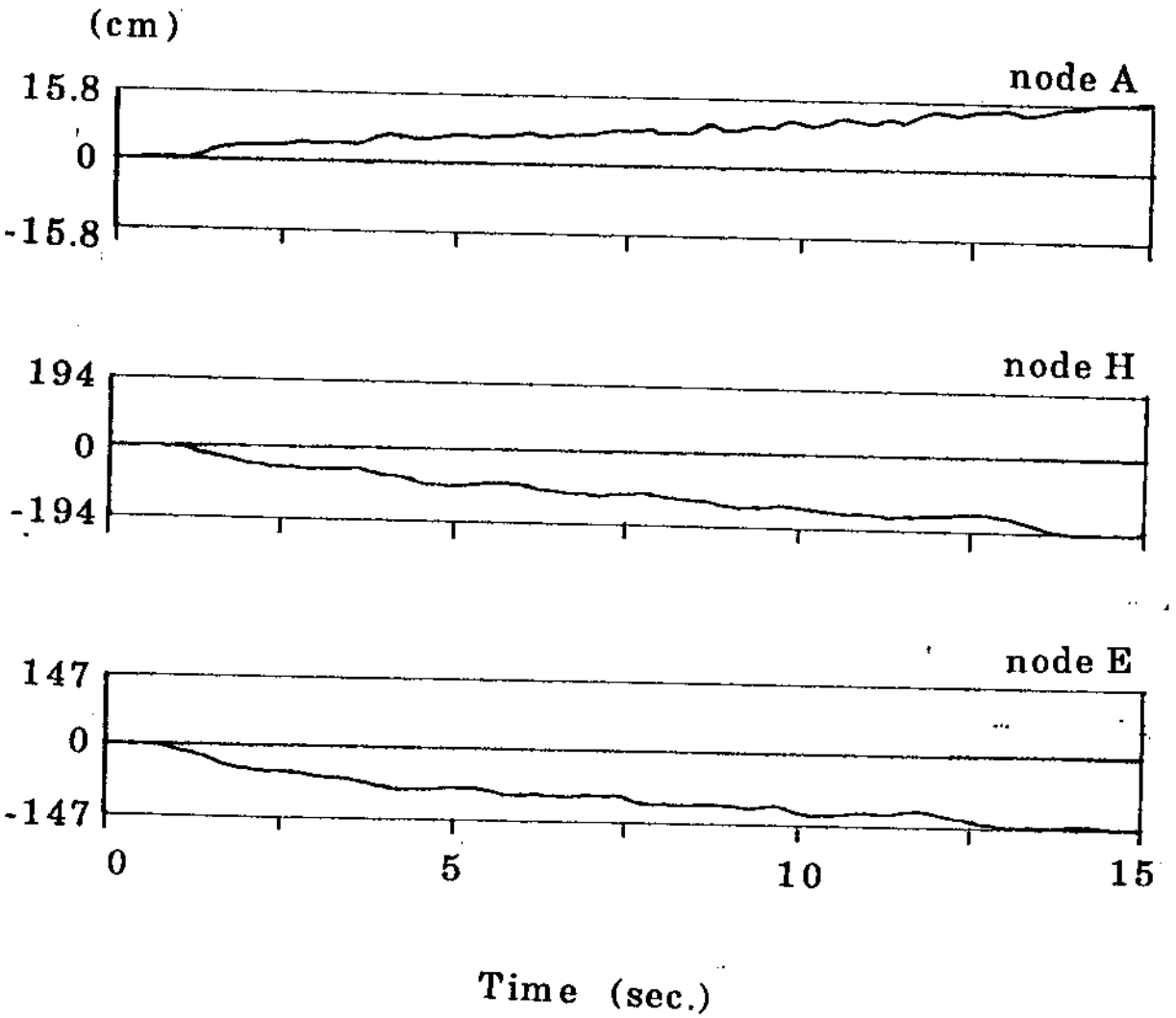

Fig. 5.5 Vertical Displacement Time Histories at Various Locations

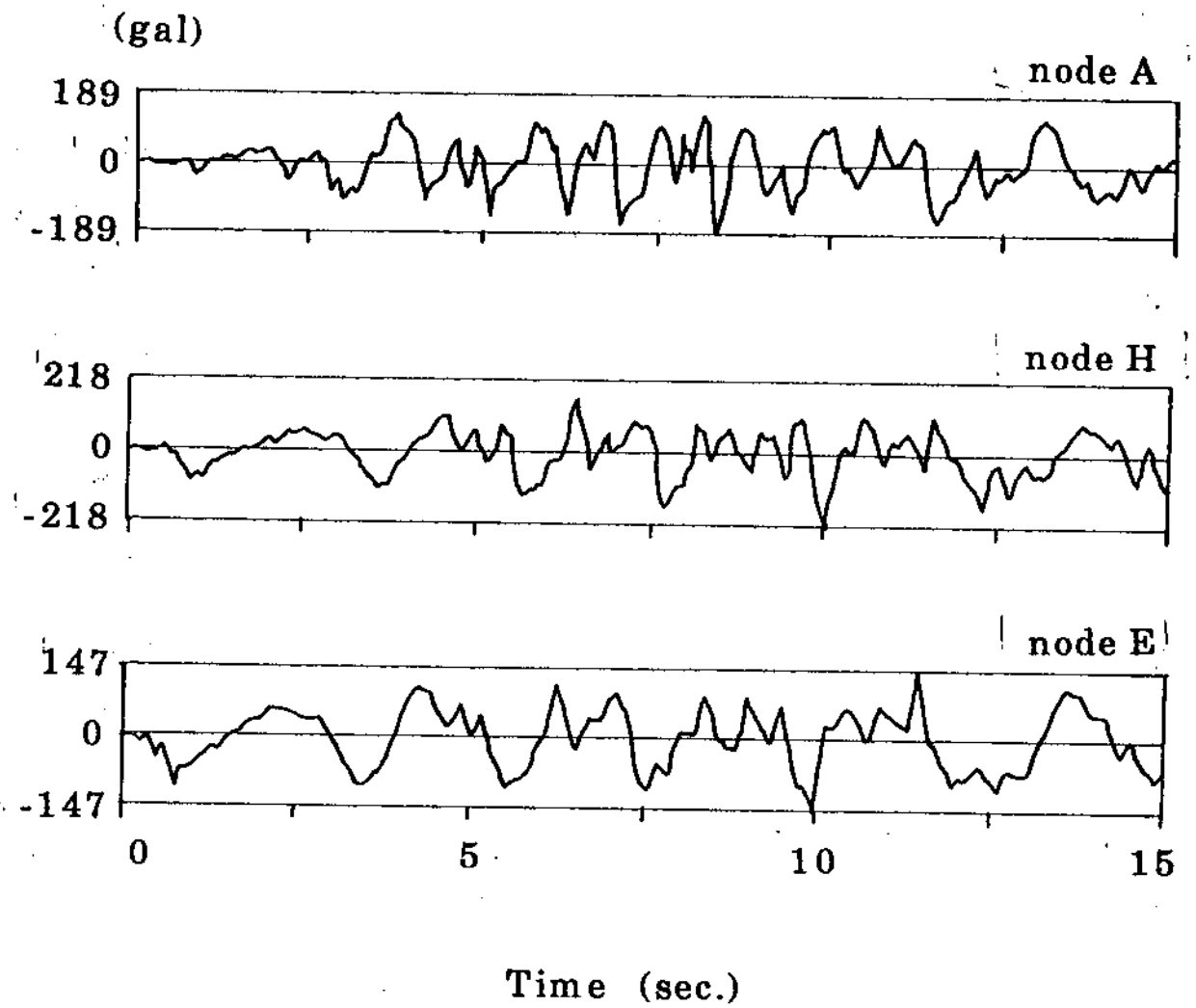

Fig. 5.6 Horizontal Acceleration Time Histories at Various Locations

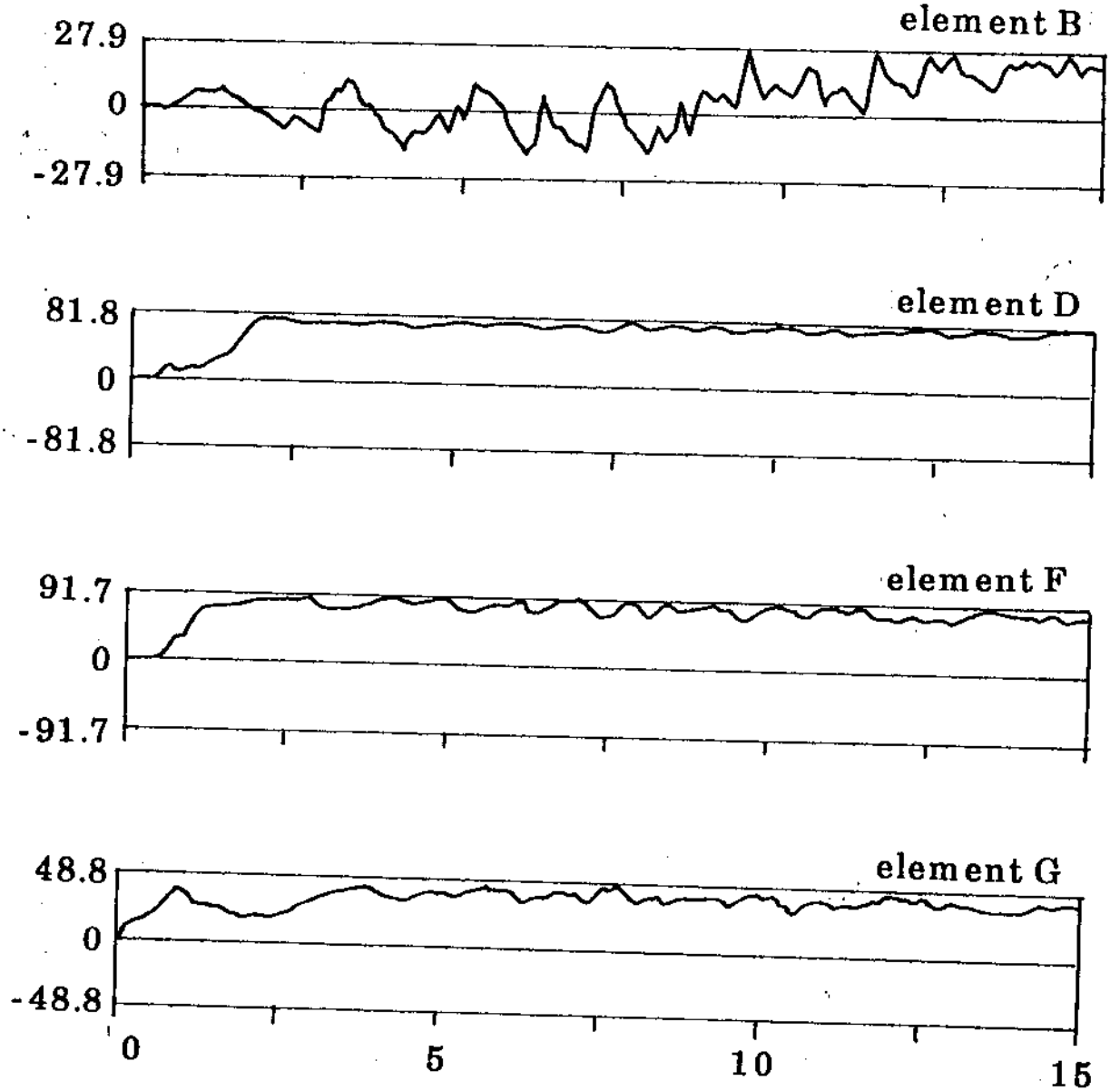

Fig. 5.7 Excess Pore Pressure Time Histories at Various Locations

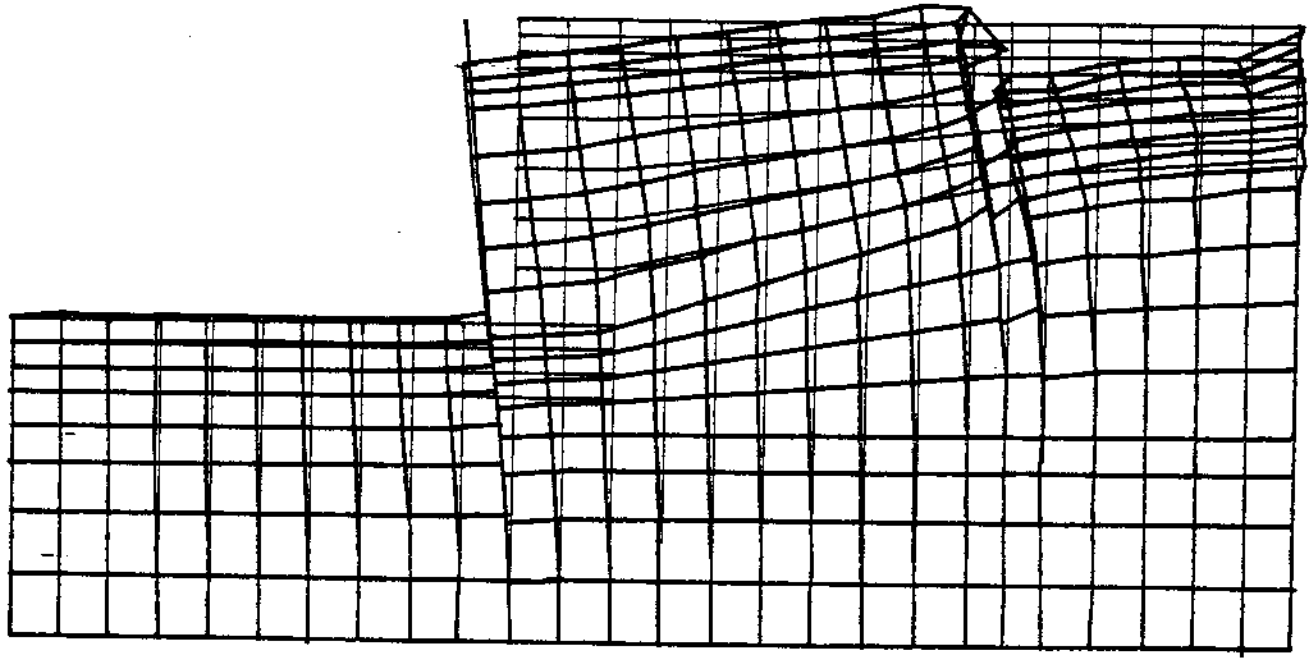

Fig. 5.8 Computed Displacements at 15 Seconds of Earthquake Shaking

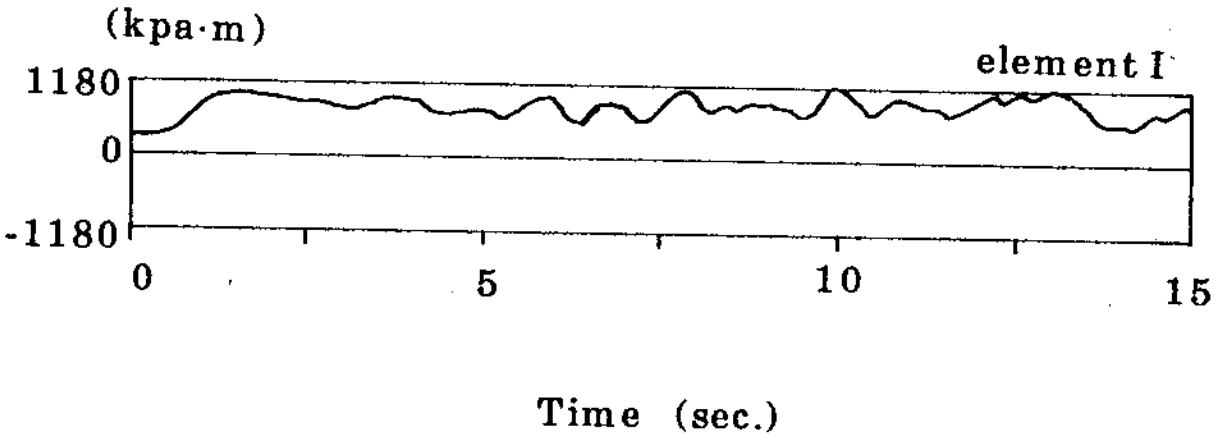

Fig. 5.9 Bending Moment Time History at 6 m below the Sea Level

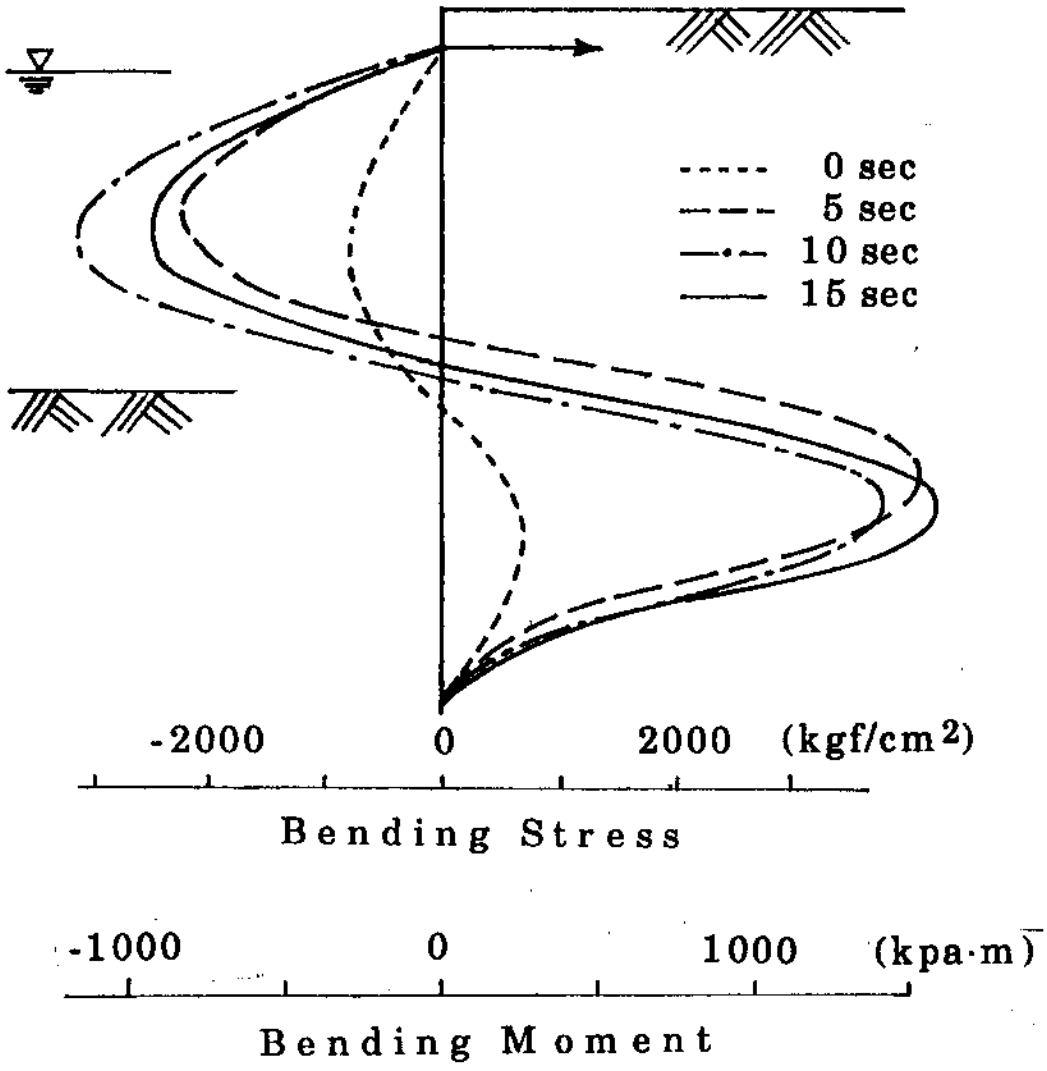

Fig. 5.10 Bending Moment Stresses Induced in Sheet Pile at Various Times

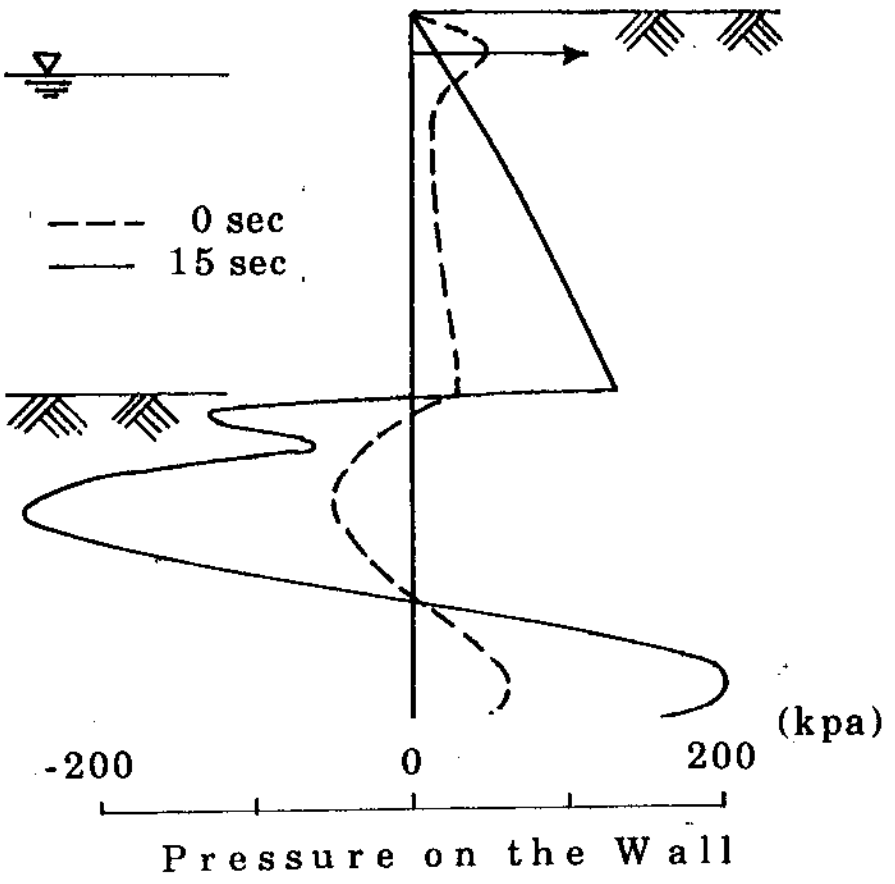

Fig. 5.11 Pressure Acting on Sheet Pile before and at 15 Seconds of Earthquake Shaking